Supporting Information to: "3'-5' crosstalk contributes to transcriptional bursting"

Massimo Cavallaro,[1,2,3,*] Mark D. Walsh,[1] Matt Jones,[1] James Teahan,[4] Simone Tiberi,[5] Bärbel Finkenstädt,[2] and Daniel Hebenstreit[1,*]

[1] *School of Life Sciences, University of Warwick, Coventry, UK*
[2] *Department of Statistics, University of Warwick, Coventry, UK*
[3] *Mathematics Institute and Zeeman Institute for Systems Biology and Infectious Disease Epidemiology Research, University of Warwick, Coventry, UK*
[4] *Department of Chemistry, University of Warwick, Coventry, UK*
[5] *Institute of Molecular Life Sciences and Swiss Institute of Bioinformatics, University of Zurich, Zurich, Switzerland*

CONTENTS

* To whom correspondence should be addressed. E-mail: d.hebenstreit@warwick.ac.uk m.cavallaro@warwick.ac.uk

S1. DESCRIPTION OF DATA

A. Flow-cytometry data

We obtained flow cytometry data (from the BD LSRFortessa™ cell analyzer and BD FACSDiva™ software) for cell lines expressing the genes *env* and HBB, in both their wild-type (WT) and mutated (mut) versions. For each gene, experimental data were collected in four replicates (8 in total), each containing groups of observations corresponding to cells stimulated with tetracycline (Tet) at concentrations of $5, 10, 20, 40, 80$, and 250 ng/mL, respectively.

Each data-set was stored in a `.fcs` format file and it was imported and pre-processed in R as an object of class `flowFrame`, which consists of an annotated data-frame class defined in the flowCore R package [1] and designed to deal with flow-cytometry data. Rows in such data frames correspond to single measurements. Each row contains the values of two fluorescence intensities that correspond to staining for mRNA and total DNA and are labeled by `R640-670/14-A` and `UV355-450/50-A`, respectively. These readings were compesated for spectral overlap with flowCore. In addition to this, the values of four scattering observations, namely `FSC.H`, `FSC.W`, `SSC.H`, and `SSC.W`, were recorded. Such observations are thought to be correlated to cell size and granularity. Values for each observation are stored in so-called "arbitrary units" (a.u.) [2].

The first task is to identify records in the data sets corresponding to either cell debris or clumps of cells, which have to be removed from subsequent analysis. We apply the robust model-based clustering approach of Ref. [3], distributed as the flowClust package [4], to identify cell populations in the data. Based on the scattering observations, the points were grouped into 3 clusters, and the set corresponding to single cells is the one with intermediate size and granularity, as suggested by the

DNA content (see Fig. S1). For the data sets where the three detected clusters overlap, points where grouped into two clusters, instead. For this second case, inspection shows that the cluster with lower size and granularity corresponds to single cells. Standard rectangle gates were applied to remove a few outlier points whose `UV355-450/50-A` reads were lower than 500. Kernel density estimates (KDE) for the populations after this sub-setting are plotted in Fig. 2 (Main Text) and Fig. S2. Technical variation affects the shapes of the distributions only for some HIV replicates, with shoulders at the lower ends sometimes merging with the main mode. The cells corresponding to the data points in the shoulders exhibit normal characteristics (in terms of cell size and DNA content) and thus probably reflect cells without mRNA. The parameter estimates, reported in section S6, appear robust with regards to the absence or presence of the shoulders save for the highest μ_Xs.

B. Control cells

For each replicate k, we consider control cells, where the gene of interest has been deleted (see *Main text*). Such control cells were subjected to the same staining procedure as the others, which leaves a background of fluorescence probes that are not specifically bound to the mRNA. We argue that such background fluorescence stain are also present in the cells expressing the transgenes and contribute a term $\epsilon_i^{(k)}$ to the signal detected by the cell-analyzer channel of label `R640-670/14-A` for each cell i. The histograms of the signal from control cells appear skewed, as illustrated for example in Fig. S3 (left). We chose to fit the Azzalini's skew-normal distribution, that has PDF

$$f_\epsilon(y|a^{(k)},\mu_\epsilon^{(k)},\sigma_\epsilon^{(k)}) = 2\Phi((y-\mu_\epsilon^{(k)})\,\sigma_\epsilon^{(k)}\,a^{(k)})\,\phi(y|\mu_\epsilon^{(k)},\sigma_\epsilon^{(k)}), \quad (1)$$

to such data, where Φ and ϕ are the standard normal CDF and normal PDF, respectively, while the mean $\mu_\epsilon^{(k)}$, the standard deviation $\sigma_\epsilon^{(k)}$, and the skewness parameter $a^{(k)}$ are point estimates from the control data sets. The maximum likelihood estimates for each replicate are reported in Table S1 (see also Figs. S3(left)).

C. SmFISH and Nanostring barcoding data

Flow-FISH data are supplemented by microscopy-based single-molecule FISH counts (which we simply refer to as smFISH) and Nanostring nCounter® Technology bar-coding measurements. These assays are used to choose informative priors for the mean mRNA abundance and, in turn, to calibrate the flow-FISH readouts. Symbols $\overline{x}$, s_x^2, and $s_{\overline{x}}$ represent sample mean, sample variance, and standard error of the mean, respectively. Based on these, we chose truncated normal informative priors for the average expression level $\mu_X \sim \mathcal{N}(\overline{x}, s_{\overline{x}})$, with the constraint $\mu_X > 0$, for all replicates k.

HEK293 cells are not ideal for smFISH, since they tend to overlap when growing, producing dense clusters after dividing. A further problem with smFISH is the limited dynamic range of suitable microscopes. In fact, images tend to be overexposed when recorded during transcriptional bursts at settings that are otherwise optimal for lower transcript numbers and, conversely, optimal settings for transcriptional bursts do not cope well when transcript numbers are low. Therefore we only exploit smFISH results to infer the average expression level, and rely on flow-FISH to study the noise. SmFISH data yield the summary statistics of Table S2 for the mean expression of HBB. Nanostring data (*SI Dataset 1*) yields the summary statistics of Table S3 for the mean expression of *env*.

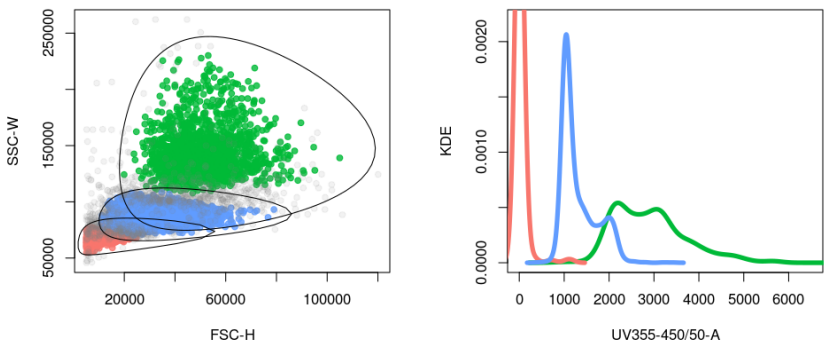

FIG. S1. Clustering of flow-cytometry data. (left) Clusters are projected to the `FSC.W-SSC.H` plane and plotted with the ellipses that delimit the 0.60 quantiles of fitted t-distributions. (right) Inspection of `UV355-450/50-A` shows signature distributions for DNA content, thus suggesting that the central cluster (in blue color) contains single-cell reads. Duplets have twice the amount of DNA content than single cells.

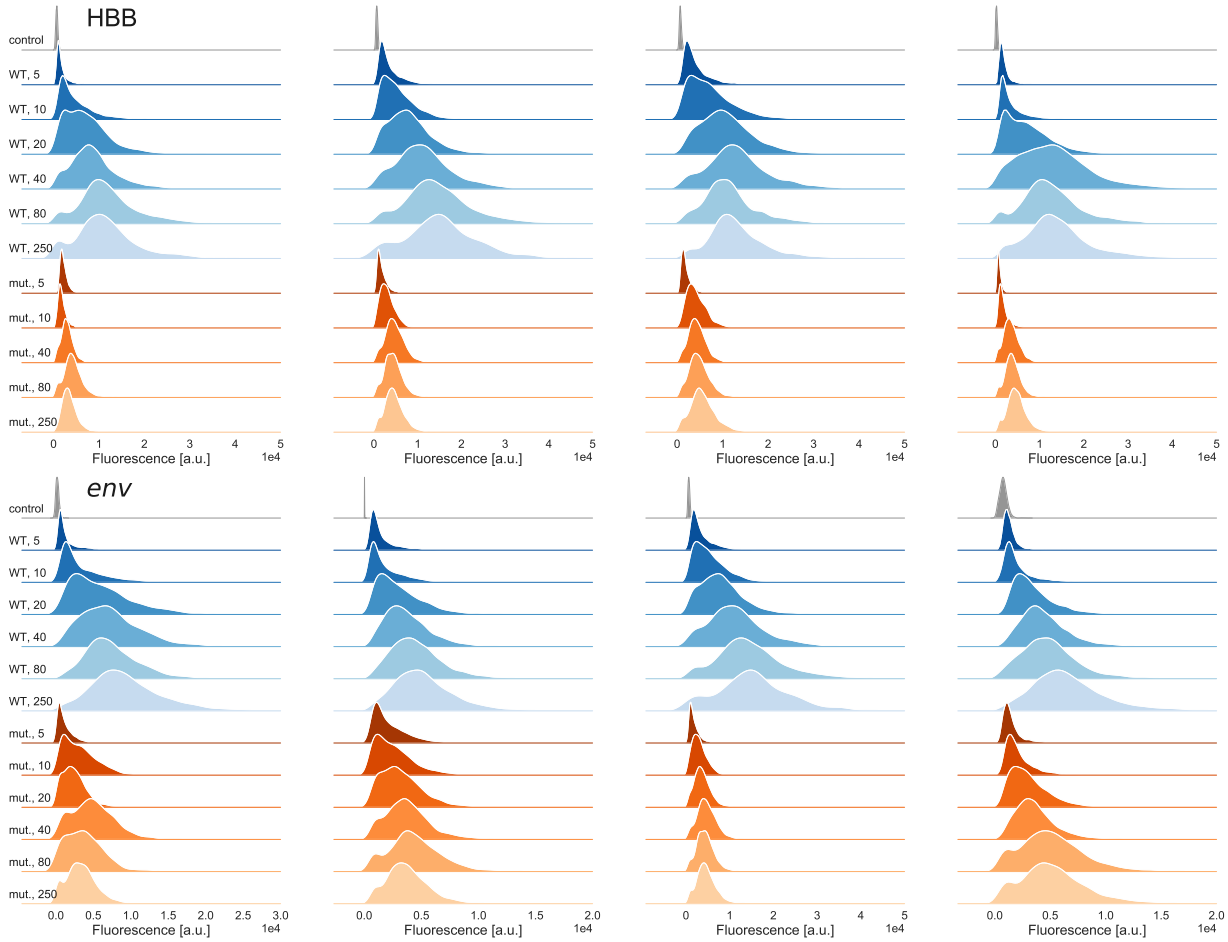

FIG. S2. KDEs of the flow-FISH single-cell readings corresponding to the abundances of HBB (top) and *env* (bottom) transcripts, from wild-type (blue), mutant (orange), and control (gray) cells, from 4 replicates per transgene, $k = 1, 2, 3, 4$ (left to right), at the different induction level (Tet concentrations in unit of ng/mL, shades of colors). Gene expression saturates upon increasing Tet concentration and mutant-cell expressions is lower than the wild-type. Fluorescence is given in arbitrary units (a.u.), y-axes are not to scale.

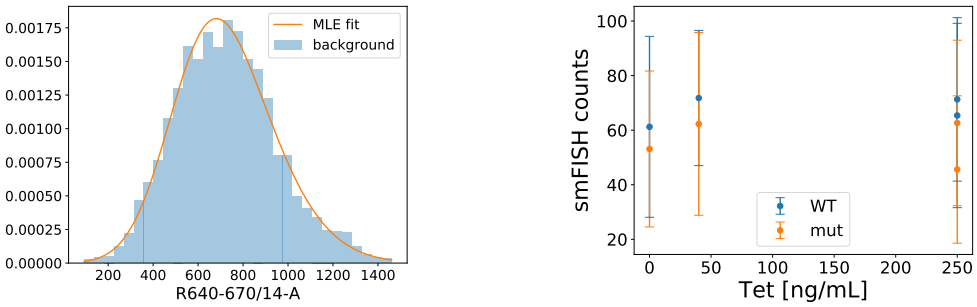

FIG. S3. Control measurements. (left) The MLE skew-normal density (line) of the background data for Tet=40 ng/mL, $k = 1$, WT, is in good agreement with the empirical histogram. (right) Microscopy FISH count summary of housekeeping gene Akt1 vs induction levels, for both wild-type and mutant cells. Points and error bars are sample means and standard deviations, respectively.

TABLE S1. MLE estimation of the control-cell fluorescence (replicates 2 (HBB) and 4 (HIV) have the same background parameters as measurements were performed the same day with the same control cells).

gene	k	Tet	$\mu^{(k)}$	$\sigma^{(k)}$	$a^{(k)}$	$s_\mu^{(k)}$	$s_\sigma^{(k)}$	$s_a^{(k)}$
HBB	1	0	389.504	348.098	1.817	15.670	12.396	0.214
HBB	1	250	514.828	307.460	1.632	11.667	9.027	0.153
HBB	2	0	625.804	458.715	1.863	21.687	17.915	0.230
HBB	2	250	459.139	311.688	2.075	9.098	7.703	0.169
HBB	3	0	539.613	360.195	2.046	11.838	10.270	0.182
HBB	3	250	493.913	337.605	2.091	10.440	9.088	0.178
HBB	4	0	53.140	320.685	2.303	7.201	6.514	0.151
HBB	4	250	112.667	256.183	1.748	5.507	4.497	0.094
HIV	1	0	565.327	390.016	1.834	8.397	6.936	0.102
HIV	1	250	443.898	463.603	1.813	14.774	12.117	0.148
HIV	2	0	-31.395	230.794	1.108	13.129	8.356	0.145
HIV	2	250	-23.282	312.375	2.066	8.109	7.156	0.145
HIV	3	0	196.970	401.184	5.423	6.238	8.517	0.425
HIV	3	250	407.813	259.586	1.445	16.865	12.125	0.226
HIV	4	0	625.804	458.715	1.863	21.687	17.915	0.230
HIV	4	250	459.139	311.688	2.075	9.098	7.703	0.169

TABLE S2. Summary statistics for the mean expression of HBB, obtained from microscopy FISH.

gene	Tet	$\overline{x}$	s_x^2	sample size
WT	0	64.868	2984.538	585
WT	5	115.450	7640.059	202
WT	10	175.150	18093.547	193
WT	20	312.945	32327.429	347
WT	40	384.111	23962.077	190
WT	80	414.105	31613.582	437
WT	250	565.351	54765.760	342
mut	0	38.953	1431.185	379
mut	5	41.645	717.115	279
mut	10	62.995	3573.429	198
mut	40	90.709	3301.445	468
mut	80	115.413	7096.164	179
mut	250	163.547	7375.582	892

TABLE S3. Summary statistics for the mean expression of HIV, obtained from nCounter® data. The standard error of the mean $s_{\overline{x}}^2$ is obtained propagating the errors from the nCounter® and the Atk1 smFISH measurements used for normalisation.

gene	Tet	$\overline{x}$	$s_{\overline{x}}^2$
WT	0	24.723	3.247
WT	5	72.975	3.247
WT	10	115.872	3.247
WT	20	151.462	3.247
WT	40	199.433	3.247
WT	80	232.644	3.247
WT	250	238.178	3.247
mut	0	21.875	3.247
mut	5	36.842	3.247
mut	10	58.108	3.247
mut	20	95.460	3.247
mut	40	139.979	3.247
mut	80	162.874	3.247
mut	250	187.287	3.247

S2. PHENOMELOGICAL GENE EXPRESSION MODELS

We describe the gene expression in terms of the standard phenomenological two-state model [5]. This model assumes that the gene randomly alternates between an "on" and an "off" state, and that the mRNA is only transcribed, at rate $\tilde{\alpha}$, during the on state. The gene switches from "off" to "on" and from "on" to "off" states after an exponentially distributed random time with mean $1/k_{\text{on}}$ and $1/k_{\text{off}}$, respectively. Consequently, the transcriptional bursting is fully characterised by the rates $\tilde{\alpha}$, $\tilde{k}_{\text{on}}$, and $\tilde{k}_{\text{off}}$. In addition to this, mRNA is degraded at rate $\tilde{d}$. It is convenient to express the rates in units of the inverse of the mean mRNA life-time $\tilde{d}$, i.e.,

$$\tilde{k}_{\text{off}} = k_{\text{off}}\,\tilde{d}, \tag{2}$$

$$\tilde{k}_{\text{on}} = k_{\text{on}}\,\tilde{d}, \tag{3}$$

$$\tilde{\alpha} = \alpha\,\tilde{d}. \tag{4}$$

It can be shown that the stationary probability density function (PDF) of the mRNA population x for this model is (see, e.g., Ref. [6])

$$f_X(x|\alpha, k_{\text{on}}, k_{\text{off}}) = \frac{\alpha^x \mathrm{e}^{-\alpha}\,\Gamma(k_{\text{on}}+x)\Gamma(k_{\text{on}}+k_{\text{off}})}{x!\,\Gamma(k_{\text{on}}+k_{\text{off}}+x)\,\Gamma(k_{\text{on}})}\,{}_1F_1(k_{\text{off}}, k_{\text{on}}+k_{\text{off}}+x; \alpha), \tag{5}$$

where Γ is the gamma function and ${}_1F_1$ is the confluent hyper-geometric function of the first kind. An alternative representation of the PDF (5) is

$$f_X(x|\alpha, k_{\text{on}}, k_{\text{off}}) = \int_0^1 f_{\text{Poi}}(x|\alpha p) f_{\text{Be}}(p|k_{\text{on}}, k_{\text{off}})\,\mathrm{d}p, \tag{6}$$

where

$$f_{\text{Poi}}(x|\alpha) = \frac{\alpha^x \mathrm{e}^{-\alpha}}{x!}, \tag{7}$$

$$f_{\text{Be}}(p|k_{\text{on}}, k_{\text{off}}) = p^{k_{\text{on}}-1}(1-p)^{k_{\text{off}}-1}\frac{\Gamma(k_{\text{on}}+k_{\text{off}})}{\Gamma(k_{\text{off}})\Gamma(k_{\text{on}})}, \tag{8}$$

are density distributions of Poisson and beta random variables (RVs), respectively.

The PDF of equation (6) encodes the following hierarchy

$$X|\alpha, P \sim \text{Poi}(\alpha P), \tag{9}$$

$$P|k_{\text{on}}, k_{\text{off}} \sim \text{Beta}(k_{\text{on}}, k_{\text{off}}). \tag{10}$$

Further details can be found, e.g., in Refs. [6, 7]. It is convenient to reparametrise the Poisson-beta distribution in terms of its mean

$$\mu_X = \alpha\frac{k_{\text{on}}}{k_{\text{off}}+k_{\text{on}}}, \tag{11}$$

to get

$$X|\mu_X, k_{\text{on}}, k_{\text{off}}, P \sim \text{Poi}(\mu_X\frac{k_{\text{off}}+k_{\text{on}}}{k_{\text{on}}}P), \tag{12}$$

$$f_X(x|\alpha, k_{\text{on}}, k_{\text{off}}) =: f'_X(x|\mu_X, k_{\text{on}}, k_{\text{off}}). \tag{13}$$

In fact, this allows us to exploit knowledge on μ_X in the form of informative priors of S1 C. The expression for the squared coefficient of variation (CV^2) can also be written in terms of μ_X, i.e.,

$$\text{CV}_X^2 = \frac{1}{\mu_X} + \frac{k_{\text{off}}}{k_{\text{on}}(1+k_{\text{off}}+k_{\text{on}})}, \tag{14}$$

where the second term on the r.h.s. quantifies the overdispersion of X with respect to a Poisson random variable. Such a functional relation between CV_X^2 and μ_X has been encountered in gene expression data [8–12]. The probability P cannot be directly accessed and therefore is a latent (hidden) variable for the model. In fact, for our data, the mRNA number is a latent variable too, being only inferred from the measured fluorescence signals. This can be encoded into a measurement equation, as explained in the next section.

In the limit as $k_{\mathrm{off}} \to \infty$, $\alpha \to \infty$, with the ratio α/k_{off} held fixed, the population mean and CV^2 satisfy

$$\mu_X = \frac{\alpha}{k_{\mathrm{off}}} k_{\mathrm{on}}, \tag{15}$$

$$\mathrm{CV}_X^2 = \frac{1}{\mu_X} + \frac{1}{k_{\mathrm{on}}}, \tag{16}$$

respectively, while the distribution of X approaches the negative binomial distribution with PDF

$$f''_X(x|\mu_X, k_{\mathrm{on}}) = \frac{\Gamma(k_{\mathrm{on}}+x)}{x!\,\Gamma(k_{\mathrm{on}})} \left(\frac{k_{\mathrm{on}}}{k_{\mathrm{on}}+\mu_X}\right)^{k_{\mathrm{on}}} \left(\frac{\mu_X}{k_{\mathrm{on}}+\mu_X}\right)^{x}. \tag{17}$$

This can be easily proven using the Poisson-gamma mixture formulation of the negative binomial RV X, i.e.,

$$X|\lambda \sim \mathrm{Poi}(\lambda), \tag{18}$$

$$\lambda|k_{\mathrm{on}}, k_{\mathrm{off}}/\alpha \sim \mathrm{Gamma}(k_{\mathrm{on}}, k_{\mathrm{off}}/\alpha). \tag{19}$$

In fact, the beta distribution scaled by $\alpha > 0$ approaches the gamma distribution as $k_{\mathrm{off}} \to \infty$, $\alpha \to \infty$, i.e.,

$$\frac{1}{\alpha}\frac{\Gamma(k_{\mathrm{on}}+k_{\mathrm{off}})}{\Gamma(k_{\mathrm{on}})\Gamma(k_{\mathrm{off}})} \left(\frac{x}{\alpha}\right)^{k_{\mathrm{on}}-1} \left(1-\frac{x}{\alpha}\right)^{k_{\mathrm{off}}-1} \asymp \frac{\frac{k_{\mathrm{off}}}{\alpha}^{k_{\mathrm{on}}}\, x^{k_{\mathrm{on}}-1}\, \mathrm{e}^{-\frac{k_{\mathrm{off}}}{\alpha}x}}{\Gamma(k_{\mathrm{on}})}, \tag{20}$$

which follows from known asymptotic relations

$$\lim_{k_{\mathrm{off}}\to\infty} \frac{\Gamma(k_{\mathrm{off}}+k_{\mathrm{on}})}{\Gamma(k_{\mathrm{off}}){k_{\mathrm{off}}}^{k_{\mathrm{on}}}} = 1, \tag{21}$$

$$\lim_{\alpha\to\infty} \left(1-\frac{x}{\alpha}\right)^{\alpha\frac{k_{\mathrm{off}}}{\alpha}} = \mathrm{e}^{-\frac{k_{\mathrm{off}}}{\alpha}x}. \tag{22}$$

The ratio α/k_{off} has a simple interpretation, being the expected number of transcription events during an on phase. In Ref. [13] this ratio has been referred to as the "expected burst size". In the limit as $k_{\mathrm{on}} \to \infty$ with the mean expression μ_X held fixed, the negative binomial distribution (17) approaches the distribution

$$f'''_X(x|\mu_X) := f_{\mathrm{Poi}}(x|\mu_X). \tag{23}$$

S3. MEASUREMENT AND TECHNICAL ERROR MODEL

The DB FACSDiva$^{\mathrm{TM}}$ software manual [14] specifies that the light intensity from fluorescent dyes is amplified linearly within a wide range (see also, e.g., Refs. [9, 15]). Based on this, we assume that the measured fluorescence Y_i of cell i is proportional to the true mRNA abundance X_i and therefore can be expressed as in the following "measurement" equation,

$$Y_i^{(k)} = \epsilon_i^{(k)} + \kappa^{(k)} X_i^{(k)}, \tag{24}$$

where k indexes the replicate, κ can be thought of as a scale and ϵ_i is the zero of such a scale, also corresponding to the background of unspecific staining and auto-fluorescence of the ith cell [7].

The dispersion of biological data is typically due to both technical errors, caused by the measurement process, and the variability intrinsic to the underlying biology. In our measurement model, for the variables $X_i^{(k)}$ to best accommodate the true biological noise of $Y_i^{(k)}$, it is important that $\epsilon_i^{(k)}$ and $\kappa^{(k)}$ are specified with sufficient precision and accuracy.

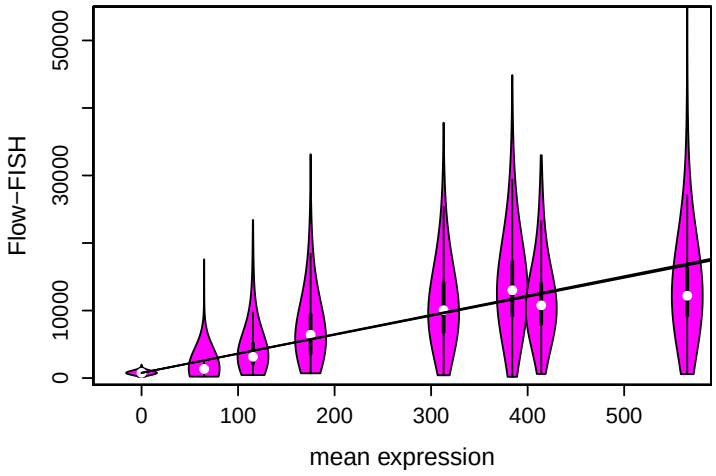

FIG. S4. Flow-FISH data (violin plots [16]) vs mean expression levels obtained from FISH data for the replicate $k = 3$, WT HBB gene. Their relation is captured by a linear model with coefficient κ.

Informative priors for $\epsilon_i^{(k)}$ are chosen according to section S1 B, i.e.,

$$\epsilon_i^{(k)} \sim \mathrm{SN}(a^{(k)}, \mu_\epsilon^{(k)}, \sigma_\epsilon^{(k)}), \tag{25}$$

where the parameters $a^{(k)}$, $\mu_\epsilon^{(k)}$, and $\sigma_\epsilon^{(k)}$ are estimated from the control cells at 250 ng/mL Tet. The standard errors of the maximum likelihood estimates are neglected. As a consequence, all the single-cell measurements can be thought of as being subjected to the same random background, thus mitigating tractability issues. For a more comprehensive fully-Bayesian hierarchical approach see Ref. [7].

To pin down informative priors for $\kappa^{(k)}$, we perform gamma regression. For each flow-FISH data-set, 500 random cell readings are selected for the main Monte Carlo estimation of section S4. The remaining reads are used as response variables for a gamma regression with identity link. Covariates are mean expression level point estimates from section S1 C. As an example, this is illustrated in Fig. S4 for $k = 3$, WT HBB gene. The GLM estimates of the expected values μ'_κ along with the standard errors s'_κ are reported in Table S4. Our prior choice is the truncated normal RV

$$\kappa \sim \mathcal{N}(\mu'_\kappa, s'_\kappa), \tag{26}$$

with the constraint $\kappa > 1$, where the mean μ'_κ and standard deviation s'_κ are obtained from the 16 values in Table S4 according to the laws of total expectation and variance, respectively, i.e.,

$$\mu'_\kappa = \overline{\mu_\kappa}, \qquad {s'}_\kappa^2 = \overline{s_\kappa^2} + \overline{\mu_\kappa^2} - \overline{\mu_\kappa}^2, \tag{27}$$

where the bar notation represents averages.

For the remaining parameters we assume

$$k_{\mathrm{on}} \sim \mathrm{Gamma}(\alpha_{k_{\mathrm{on}}}, \beta_{k_{\mathrm{on}}}), \tag{28}$$

$$k_{\mathrm{off}} \sim \mathrm{Gamma}(\alpha_{k_{\mathrm{off}}}, \beta_{k_{\mathrm{off}}}), \tag{29}$$

$$\alpha_{k_{\mathrm{on}}} = \beta_{k_{\mathrm{on}}} = \alpha_{k_{\mathrm{off}}} = \beta_{k_{\mathrm{off}}} = 0.001, \tag{30}$$

which is a classical choice for vague priors with positive support [17].

Since the replicates are independent, the likelihood of the parameters of the Poisson-beta model, for a data-set of N measurements $y_{1:N}^{(k)}$, is

$$\mathcal{L}'_k(y_{1:N}^{(k)}|\theta^{(k)}, \mu_X, k_{\mathrm{on}}, k_{\mathrm{off}}) = \prod_{j=1}^{N} \left(\sum_x f_\epsilon(y_j^{(k)} - \kappa x | a^{(k)}, \mu_\epsilon^{(k)}, \sigma_\epsilon^{(k)}) f'_X(x|\mu_X, k_{\mathrm{on}}, k_{\mathrm{off}}) \right), \tag{31}$$

TABLE S4. Estimated coefficients (means and standard errors of the mean, $\mu_\kappa^{(k)}$ and $s_\kappa^{(k)}$, respectively) of the gamma GLM.

k	gene	$\mu_\kappa^{(k)}$	$s_\kappa^{(k)}$
1	HBB WT	20.904	0.230
2	HBB WT	27.080	0.283
3	HBB WT	28.394	0.241
4	HBB WT	21.631	0.244
1	HBB mut	20.308	0.233
2	HBB mut	29.621	0.402
3	HBB mut	32.267	0.353
4	HBB mut	26.612	0.322
1	HIV WT	17.715	0.153
2	HIV WT	34.771	0.341
3	HIV WT	17.118	0.183
4	HIV WT	50.748	0.547
1	HIV mut	23.035	0.219
2	HIV mut	32.463	0.381
3	HIV mut	26.951	0.296
4	HIV mut	25.487	0.300

where $\theta^{(k)} := (\kappa, a^{(k)}, \mu_\epsilon^{(k)}, \sigma_\epsilon^{(k)})$ is the vector of the parameters that describe the experimental setting. This completes the definition of the first Bayesian model for the observed data. The directed acyclic graph (DAG) of the full posterior of this model is illustrated in Fig. S5(A).

Consistently, the likelihood of the parameters of the negative-binomial model is

$$\mathcal{L}''_k(y^{(k)}_{1:N}|\theta^{(k)}, \mu_X, k_{\text{on}}) = \prod_{j=1}^{N} \left(\sum_x f_\epsilon(y_j^{(k)} - \kappa x | a^{(k)}, \mu_\epsilon^{(k)}, \sigma_\epsilon^{(k)}) f''_X(x|\mu_X, k_{\text{on}}) \right), \tag{32}$$

as illustrated in Fig. S5(B). The simplest Poisson model, the likelihood is

$$\mathcal{L}'''_k(y^{(k)}_{1:N}|\theta^{(k)}, \mu_X) = \prod_{j=1}^{N} \left(\sum_x f_\epsilon(y_j^{(k)} - \kappa x | a^{(k)}, \mu_\epsilon^{(k)}, \sigma_\epsilon^{(k)}) f'''_X(x|\mu_X) \right), \tag{33}$$

whose DAG is illustrated in Fig. S5(C).

S4. MONTE CARLO ESTIMATION

A. MCMC samplers

Adaptive Metropolis–Hastings samplers to fit the model to the data where implemented using the PyMC library for probabilistic programming [18], version `2.3.7`, which has a flexible object oriented syntax and provides tools to handle long traces and perform diagnostics. To improve the convergence speed, the array containing the N elements of a dataset was numerically sorted by value and split into $M = N/10$ blocks of size 10. The latent random-variable arrays $P_{1:N}$ and $X_{1:N}$ were batched too, as the RVs conditioned on the data of a single block are strongly correlated and are conveniently updated during single Metropolis–Hastings steps. Using the symbol $\mathbf{1}_x$ for the identity matrix and $\mathcal{N}_x$ to represent a multivariate normal RV of dimension x, the simulation of posterior samples for the Poisson-beta model proceeds as follows:

- For $i = 0, 1, \ldots, M$, values of the 10-value blocks $P_{(i\,10+1):(i+1)10}$ and $(X_{i\,10+1):(i+1)10}$ are updated according to a random walk Metropolis with proposals $\mathcal{N}_{10}(\mu_i^{(P)}, \sigma_i^{(P)}\,\mathbf{1}_{10})$ and $\mathcal{N}_{10}(\mu_i^{(X)}, \sigma_i^{(X)}\,\mathbf{1}_{10})$ respectively,

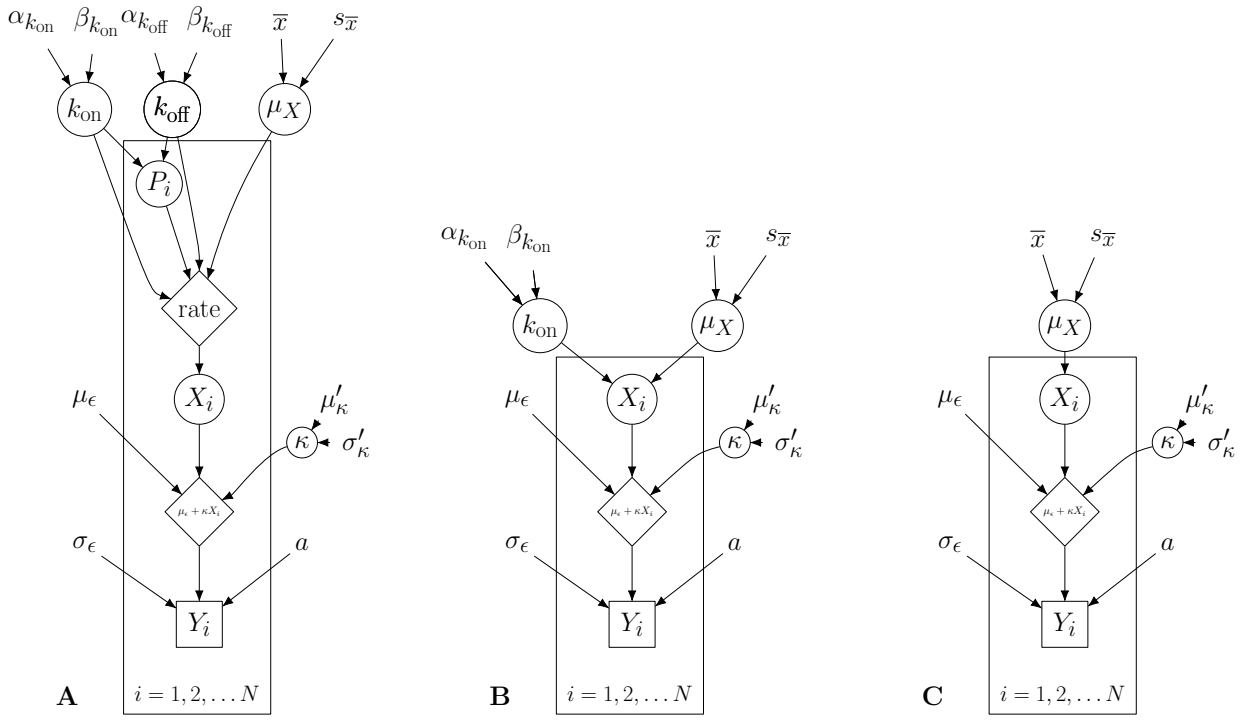

FIG. S5. DAG for the Poisson-beta model (A), the negative-binomial model (B), and the naïve Poisson model (C) with measurement equation. Circle nodes represent parameters to be estimated, blank nodes represent set parameters, diamonds correspond to deterministic functions of their parents, and square nodes represent observations.

- The RVs μ_X, κ, $k_{\rm on}$, and $k_{\rm off}$ are updated as a single block according to the adaptive Metropolis–Hastings method of Ref. [19] with proposal $\mathcal{N}_4(\mu, \Sigma)$.

The proposal parameters $\mu_i^{(X)}$, $\sigma_i^{(X)}$, $\mu_i^{(P)}$, $\sigma_i^{(P)}$, $(i = 1, \ldots, M)$, μ, and Σ are chosen adaptively. To improve the adaptation (noting that the posterior for $k_{\rm off}$ is more disperse than those of μ_X, κ, and $k_{\rm on}$), Σ is initialised to the diagonal matrix $\mathrm{diag}(0.1, 0.1, 0.1, 1)$.

In order to mitigate tractability issues (which is mainly due to the large number of presence of latent variables), the model is only fitted to a randomly sampled subset of $N = 500$ data points. For a more modern approach to cope with latent variables see Ref. [7], which also defines a more complex hierarchical model.

The sampler implemented for the negative-binomial model is similar to the one implemented for the Poisson-beta model (with data organised into M ranked batches) but converges and mixes more rapidly, as it does not encode for the latent variables P_i, $i = 1, 2, \ldots, N$. The simulation proceeds as follows:

- For $i = 0, 1, \ldots, M$, values of $X_{(i\,10+1):(i+1)\,10}$ are updated according to a random-walk Metropolis with proposal $\mathcal{N}_{10}(\mu_i^{(X)}, \sigma_i^{(X)}\,\mathbf{1}_{10})$.
- The random variables μ_X, κ and $k_{\rm on}$ are updated simultaneously according to the adaptive Metropolis–Hastings method with proposal $\mathcal{N}_3(\mu, \Sigma)$,

where the quantities $\mathbf{1}_x$, $\mu_i^{(X)}$, $\sigma_i^{(X)}$, $(i = 1, \ldots, M)$, μ, and Σ are defined as in the former case. The Poisson-model sampler is analogous to the negative binomial, except that it does not include the parameter $k_{\rm on}$. All the samplers were successfully tested with simulated data.

B. Consensus posteriors

The posterior

$$p(\vartheta | y^{(1)}_{1:N}, y^{(2)}_{1:N} y^{(3)}_{1:N}, y^{(4)}_{1:N}) \propto \prod_{k=1}^{4} \left[\mathcal{L}_k(y^{(k)}_{1:N}|\vartheta)\right] p(\vartheta) \tag{34}$$

represents the consensus belief on the vector of parameters ϑ among all the replicates $k = 1, 2, 3, 4$, with $p(\vartheta)$ being the prior. We approximate such a posterior by means of a consensus Monte Carlo approach, i.e., by running a separate MCMC on each of

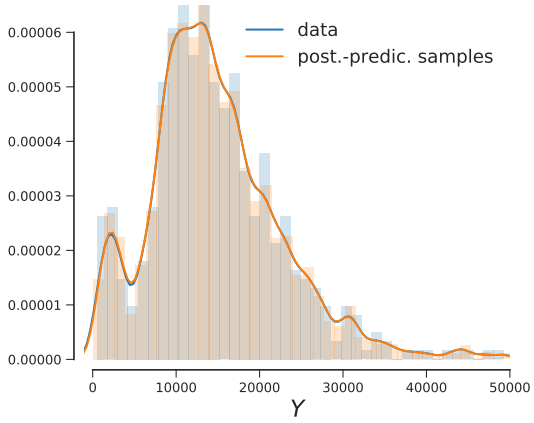

FIG. S6. KDE and histogram of the data (blue) (HBB, WT, 80 ng/mL Tet, $k = 1$) and of the draws from the corresponding posterior-predictive distribution (orange), according to the negative-binomial model. It is possible to visually appreciate their overlap. To quantify the extent to which the posterior predictive reproduces the true data distribution for all the fit, we studied the Wasserstein distance of the two distribution.

the datasets $y^{(k)}_{1:N}$, $k = 1, 2, 3, 4$, and then averaging individual Monte Carlo draws across, as in Ref. [20]. The draws $\vartheta^{(k)}_j$, $j = 1, \ldots, L$, $k = 1, 2, 3, 4$, are combined into the weighted averages

$$\vartheta_j = \frac{\sum_k \vartheta^{(k)}_j w_{(k)}}{\sum_k w_{(k)}}, \tag{35}$$

where $w_{(k)}$ is the vector of the reciprocal of the marginal posterior variances. This method has been only justified rigorously for Gaussian posteriors and only yields approximate posteriors, in general. However, it allowed us to distribute the Bayesian analysis across different machines , and therefore was of great utility to aggregate results.

C. Goodness of fit

To evaluate the goodness of fit (GoF) we estimate the posterior predictive distribution

$$p(\tilde{y}^{(k)}_{1:N}|y^{(k)}_{1:N}) = \int p(\tilde{y}^{(k)}_{1:N}|\theta)p(\theta|y^{(k)}_{1:N})\,\mathrm{d}\theta, \tag{36}$$

where θ is the vector of all parameters, by generating pseudo-data $\tilde{y}^{(k)}_{1:N}$ for the model using the parameters drawn from the posterior $p(\theta|y^{(k)}_{1:N})$ alongside each MCMC chain. A GoF test follows by measuring to what extent the pseudo-data deviate from $y^{(k)}_{1:N}$. Specifically, we calculate the root mean square displacement (RMSD) of the data $y^{(k)}_i$, $i = 1, \ldots, N$ with respect to the sample mean $\bar{y}^{(k)}_i$ of the draws from the marginal posterior predictive, i.e.,

$$\mathrm{RMSD}(\bar{y}^{(k)}_{1:N}, y^{(k)}_{1:N}) = \sqrt{\frac{1}{N}\sum_{i=1}^{N}(\bar{y}^{(k)}_i - y^{(k)}_i)^2}. \tag{37}$$

Comparison between the RMSD results for the Poisson-beta and the negative-binomial models is shown in Fig. S7, which suggests that both these models fit the data equally well. Conversely, the RMSDs for the Poisson model are always higher that the RMSDs for the two former models (see Fig. S7) implying that the Poisson model does not fit as well. Further, we computed the Wasserstein distance in distribution between the data and the pseudo-data. The Wasserstein distance between two distributions u and v is defined as

$$l_1(u, v) = \int_{-\infty}^{\infty} |U - V|, \tag{38}$$

where U and V are the empirical cumulative distribution functions associated to and u and v, respectively. Fig. S7 shows that the distances are always smaller than the 95% percentile of bootstrap-samples distances from the true data, thus confirming GoF. Bin sizes for the empirical distribution were chosen according to the Freedman–Diaconis rule.

S5. MRNA DECAY RATES

The draws from the posteriors of the dimensionless rates k_{on}, k_{off}, and α are converted to number of events per minute $\tilde{k}_{\mathrm{on}}$, $\tilde{k}_{\mathrm{off}}$, and $\tilde{\alpha}$ by using estimated decay rates of mRNA. For the HBB gene, decay rates were measured in Ref. [22] (and are reported in Table S5). Due to the detection of two different mRNA isoforms, viz., "rt" and "pA", the empirical mRNA distribution can be thought of a Gaussian mixture density with PDF

$$f(x) = p_{\mathrm{pA}}\,\phi(x|\mu_{\mathrm{pA}}, \sigma_{\mathrm{pA}}) + p_{\mathrm{rt}}\,\phi(x|\mu_{\mathrm{rt}}, \sigma_{\mathrm{rt}}), \tag{39}$$

$p_{\mathrm{rt}} + p_{\mathrm{rt}} = 1$, with parameters of Table S5. According to equations (2)-(4), the traces from k_{on}, k_{off}, and α were multiplied by draws from this Gaussian mixture to obtain $\tilde{k}_{\mathrm{on}}$, $\tilde{k}_{\mathrm{off}}$, and $\tilde{\alpha}$.

We measured total *env* RNA content (including non-poly-adenylated transcripts) with RT-qPCR, using gene-specific primers (forward primers bind exon 1 and reverse primers bind the 3'UTR, see section S10 C). The decay rates of *env* transcripts were obtained by fitting a linear model to the logarithm of RT-qPCR measurements of transcripts vs time in

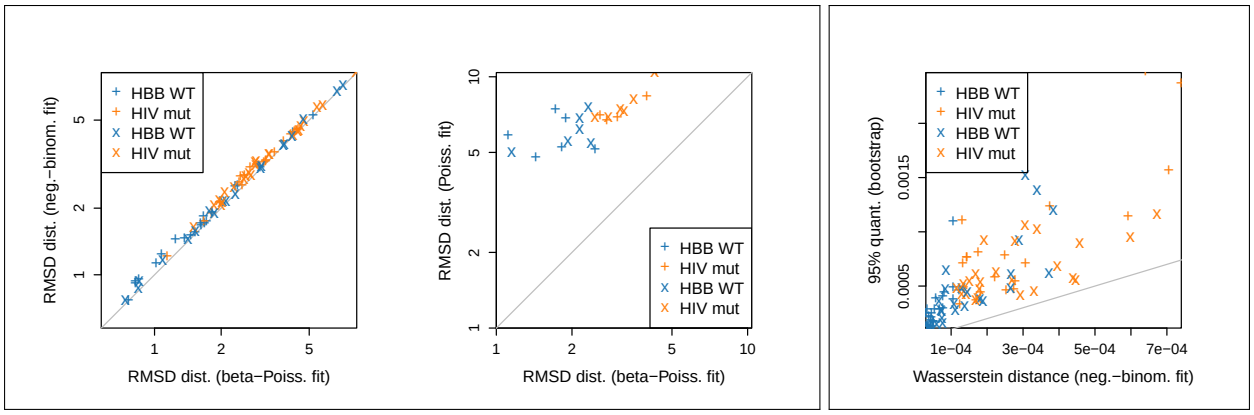

FIG. S7. GoF analysis. (left and centre) RMSDs of the data with respect to the sample means of the (posterior predictive (see eq. (37)) for each dataset. Comparison of Poisson-beta model vs the negative-binomial model (left scatter plot) shows that the two models achieve similar GoF, while the RMSDs obtained from the Poisson model are always the largest (central scatter plot). (right) Wasserstein distances between the empirical histogram of the data and the negative-binomial model posterior predictive (x-axis) is always smaller that the 95% quantiles of the bootstrapped distances from the true data, which suggests that that the posterior-predictive samples for the negative-binomial model always reproduce the true flow-FISH data (as in, e.g., Fig. S6).

TABLE S5. . Decay rates in number of events per minutes of the two mRNA isoforms for the HBB gene. "pA" and "rt" refer to polyadenylated and read-through isoforms, respectively (it is possible to foresee larger dispersion for the mutant than for the WT).

SNP	isoform	μ	σ	p
WT	pA	0.0024	0.0002	0.72
WT	rt	0.0067	0.0016	0.28
mut	pA	0.0036	0.0003	0.11
mut	rt	0.0112	0.0023	0.89

minutes. The inferred mean μ_d and standard error σ_d of the decay rates are reported in Fig. S8. The draws from the posteriors of dimensionless rates k_{on}, k_{off}, and α were converted to number of events per minute by multiplying by normal draws $\mathcal{N}(\mu_d, \sigma_d)$, with parameters listed in Fig. S8.

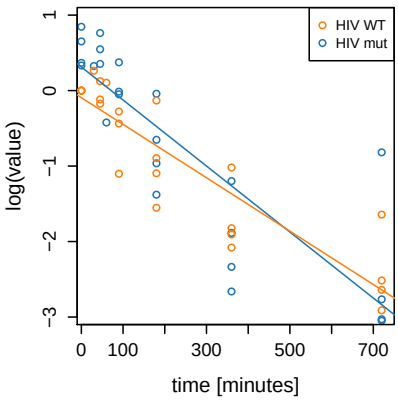

SNP	μ_d	σ_d
WT	0.0044	6e-04
mut	0.0035	4e-04

FIG. S8. Logarithm of RT-qPCR $2^{-\Delta\Delta C_t}$ measurements of residual transcripts vs time of the mutant and WT HIV gene transcripts. From linear regression, decay rates in unit of events per minutes are obtained.

S6. SUMMARY OF MCMC RESULTS

A. Poisson-beta distribution

Fig. S9 shows two results obtained from fitting the Poisson-beta model. The traces of the posterior chains from each replicate were combined according to the consensus Monte Carlo procedure (see section S4 B) to obtain a representation of the consensus belief of Fig. 3 (*Main text*). It is worth noting that the credible intervals for $\tilde{k}_{\text{off}}$ and $\tilde{\alpha}$ are very wide, while the MCMC draws of k_{off} and α appear strongly cross-correlated (see, e.g., Fig. S10), where the drawn samples form an angle $\text{arccot}(\alpha/k_{\text{off}})$ with the abscissae axis.

The 90% highest posterior density credible intervals (HPD CIs) and medians of the estimated parameters κ, μ_X, k_{on}, k_{off}, and α/k_{off} are reported in Tables S6-S10 (HBB gene) and Tables S11-S15 (HIV gene).

TABLE S6. κ of HBB gene

k	SNP	tet	low.HPD	median	upp.HPD
1	WT	5	9.559	11.257	13.031
1	WT	10	22.384	25.504	28.796
1	WT	20	18.866	20.662	22.473
1	WT	40	20.378	22.284	24.023
1	WT	80	25.675	27.393	29.289
1	WT	250	17.021	18.443	19.965
1	mut	5	32.504	35.358	38.254
1	mut	10	16.315	18.734	21.498
1	mut	40	23.342	25.416	27.553
1	mut	80	27.117	30.304	33.601
1	mut	250	17.047	18.166	19.282
2	WT	5	23.567	26.676	30.352
2	WT	10	22.676	24.647	28.696
2	WT	20	21.508	23.394	25.370
2	WT	40	25.727	27.715	29.846
2	WT	80	32.172	34.216	35.902
2	WT	250	24.276	25.938	27.678
2	mut	5	26.707	29.680	32.950
2	mut	10	31.601	36.919	41.979
2	mut	40	41.755	44.750	48.189
2	mut	80	27.094	30.426	33.609
2	mut	250	22.821	24.260	25.754
3	WT	5	25.938	29.050	32.440
3	WT	10	32.783	32.859	38.434
3	WT	20	30.479	32.865	35.207
3	WT	40	30.875	32.961	35.374
3	WT	80	25.001	26.456	28.116
3	WT	250	20.897	21.763	23.000
3	mut	5	24.799	27.457	30.501
3	mut	10	42.772	47.404	51.766
3	mut	40	35.653	38.381	41.145
3	mut	80	31.024	34.699	38.285
3	mut	250	28.080	29.963	31.857
4	WT	5	18.060	20.483	23.184
4	WT	10	17.540	19.780	22.412
4	WT	20	23.540	23.855	24.425
4	WT	40	30.582	32.931	35.604
4	WT	80	29.660	31.397	33.534
4	WT	250	23.480	25.104	26.733
4	mut	5	14.313	16.032	17.731
4	mut	10	23.044	26.306	30.166
4	mut	40	32.880	35.456	38.080
4	mut	80	28.650	31.858	35.336
4	mut	250	26.352	27.831	29.268

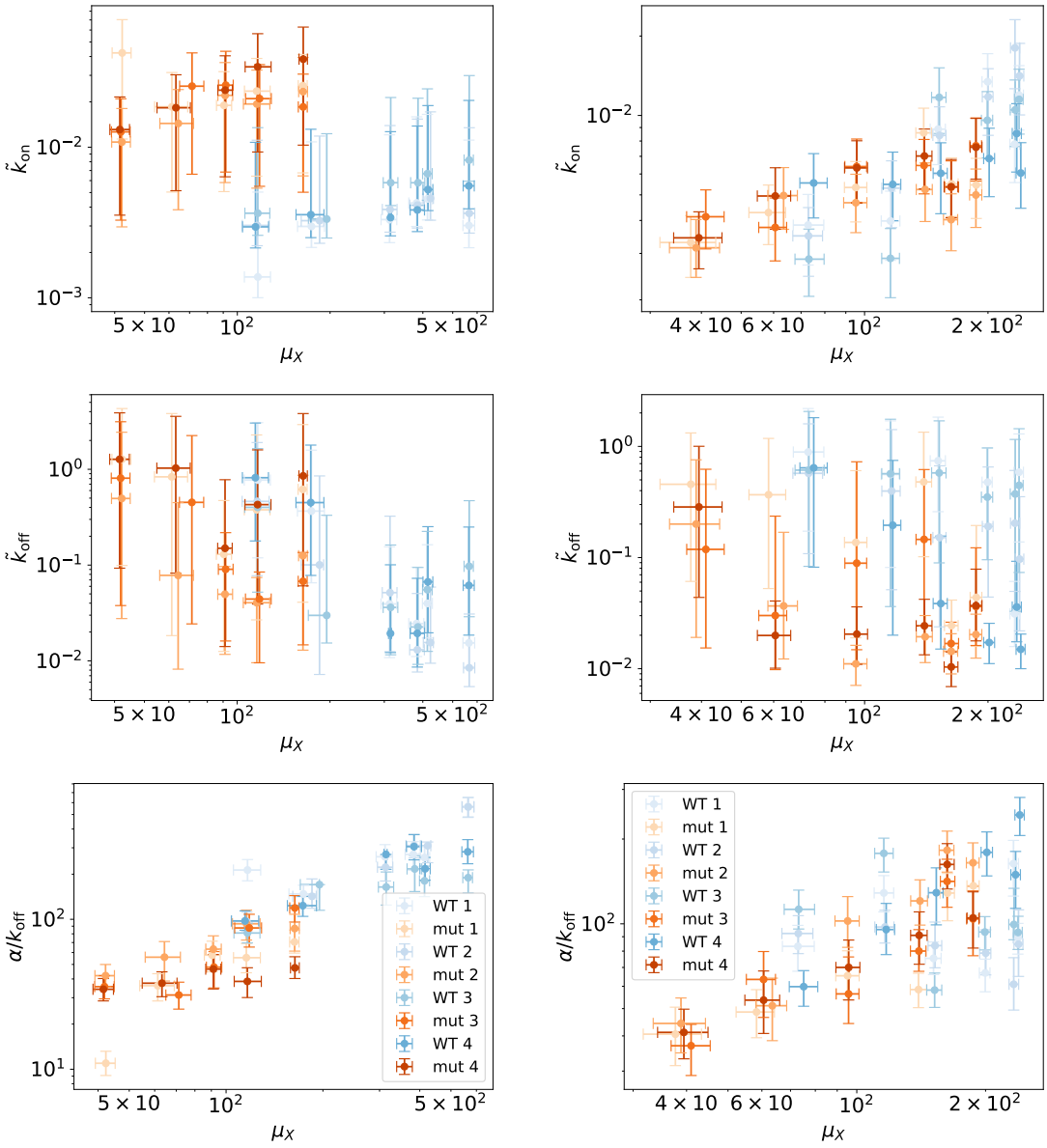

A HBB. **B** HIV.

FIG. S9. Estimates for parameters $\tilde{k}_{on}$, $\tilde{k}_{off}$, μ_X, and α/k_{off} of the Poisson- beta model, from wild-type (blue) and mutant (orange) cell data, for all induction levels, shades of colors correspond to replicates. Points are medians, error bars comprise 90% HPD CIs. HBB-gene results show results consistent across all the replicates (panel **A**). The HIB-gene results are reported in panels **B**. Increasing expression levels, three of the HIV replicates show a drop-off in the average burst size and an increase in the burst, see also Fig. S2. The consensus estimates are reported in Fig. 3, *Main text*.

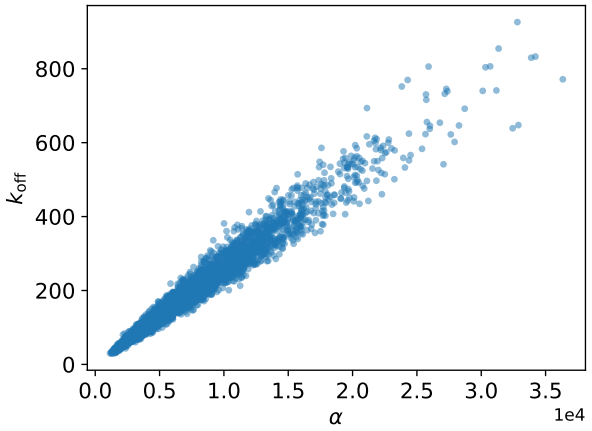

FIG. S10. Cross-correlation between the MCMC draws for the dimensionless parameters k_{off} and α.

TABLE S7. μ_X HBB

k	SNP	tet	low.HPD	median	upp.HPD
1	WT	5	105.402	116.589	128.100
1	WT	10	156.821	173.998	191.793
1	WT	20	292.726	311.989	329.181
1	WT	40	360.207	382.007	402.900
1	WT	80	398.889	414.140	429.588
1	WT	250	539.820	564.476	589.263
1	mut	5	39.239	42.300	45.212
1	mut	10	53.895	61.338	69.030
1	mut	40	85.582	90.517	95.846
1	mut	80	105.474	115.611	127.808
1	mut	250	157.627	163.197	168.546
2	WT	5	103.760	116.053	126.933
2	WT	10	161.211	184.961	190.736
2	WT	20	295.510	313.086	329.837
2	WT	40	362.581	384.120	404.709
2	WT	80	401.521	423.421	432.840
2	WT	250	542.177	565.898	589.598
2	mut	5	39.110	42.207	44.976
2	mut	10	56.058	64.338	72.119
2	mut	40	86.483	91.288	96.615
2	mut	80	104.644	115.765	127.515
2	mut	250	158.168	163.425	168.913
3	WT	5	105.803	116.504	127.453
3	WT	10	170.108	195.097	195.097
3	WT	20	297.477	314.601	331.874
3	WT	40	365.211	385.872	405.793
3	WT	80	399.257	413.887	429.090
3	WT	250	544.380	565.718	583.439
3	mut	5	39.047	41.876	44.904
3	mut	10	64.976	71.285	77.862
3	mut	40	86.882	91.723	96.974
3	mut	80	106.385	118.060	128.903
3	mut	250	157.720	163.555	168.630
4	WT	5	103.952	114.542	126.282
4	WT	10	155.066	173.247	191.033
4	WT	20	309.627	314.120	316.703
4	WT	40	363.798	383.977	404.975
4	WT	80	400.513	415.609	431.024
4	WT	250	540.749	564.065	587.349
4	mut	5	38.580	41.557	44.668
4	mut	10	54.873	63.206	70.399
4	mut	40	86.438	91.326	96.352
4	mut	80	106.004	116.457	128.697
4	mut	250	158.561	163.656	168.862

TABLE S8. $\tilde{k}_{\text{on}}$ HBB gene

k	SNP	tet	low.HPD	median	upp.HPD
1	WT	5	0.001	0.001	0.005
1	WT	10	0.002	0.003	0.011
1	WT	20	0.002	0.003	0.012
1	WT	40	0.003	0.004	0.016
1	WT	80	0.003	0.005	0.016
1	WT	250	0.002	0.003	0.011
1	mut	5	0.012	0.042	0.072
1	mut	10	0.005	0.018	0.031
1	mut	40	0.005	0.019	0.032
1	mut	80	0.006	0.023	0.038
1	mut	250	0.007	0.026	0.042
2	WT	5	0.002	0.003	0.011
2	WT	10	0.002	0.003	0.012
2	WT	20	0.003	0.004	0.014
2	WT	40	0.003	0.004	0.015
2	WT	80	0.003	0.005	0.016
2	WT	250	0.003	0.004	0.013
2	mut	5	0.003	0.011	0.018
2	mut	10	0.004	0.014	0.024
2	mut	40	0.005	0.022	0.037
2	mut	80	0.006	0.019	0.032
2	mut	250	0.006	0.024	0.039
3	WT	5	0.003	0.004	0.013
3	WT	10	0.002	0.003	0.012
3	WT	20	0.004	0.006	0.021
3	WT	40	0.004	0.006	0.021
3	WT	80	0.005	0.007	0.025
3	WT	250	0.006	0.008	0.031
3	mut	5	0.003	0.013	0.021
3	mut	10	0.007	0.026	0.042
3	mut	40	0.007	0.026	0.044
3	mut	80	0.006	0.021	0.035
3	mut	250	0.005	0.018	0.031
4	WT	5	0.002	0.003	0.011
4	WT	10	0.002	0.004	0.013
4	WT	20	0.003	0.003	0.012
4	WT	40	0.003	0.004	0.014
4	WT	80	0.004	0.005	0.019
4	WT	250	0.004	0.006	0.020
4	mut	5	0.003	0.013	0.021
4	mut	10	0.005	0.018	0.031
4	mut	40	0.006	0.024	0.040
4	mut	80	0.009	0.034	0.057
4	mut	250	0.010	0.038	0.063

TABLE S9. $\tilde{k}_{\text{off}}$ HBB gene

k	SNP	tet	low.HPD	median	upp.HPD
1	WT	5	0.125	0.765	3.017
1	WT	10	0.072	0.380	1.567
1	WT	20	0.012	0.039	0.154
1	WT	40	0.011	0.024	0.094
1	WT	80	0.016	0.040	0.161
1	WT	250	0.009	0.015	0.056
1	mut	5	0.073	1.278	4.126
1	mut	10	0.050	0.832	3.991
1	mut	40	0.013	0.130	0.474
1	mut	80	0.031	0.375	2.323
1	mut	250	0.042	0.622	3.073
2	WT	5	0.083	0.468	1.868
2	WT	10	0.004	0.103	0.843
2	WT	20	0.011	0.052	0.334
2	WT	40	0.007	0.013	0.048
2	WT	80	0.010	0.016	0.057
2	WT	250	0.005	0.008	0.031
2	mut	5	0.024	0.496	2.425
2	mut	10	0.006	0.077	0.442
2	mut	40	0.011	0.050	0.095
2	mut	80	0.010	0.040	0.073
2	mut	250	0.012	0.127	0.909
3	WT	5	0.050	0.399	1.601
3	WT	10	0.013	0.030	0.343
3	WT	20	0.011	0.035	0.156
3	WT	40	0.010	0.022	0.104
3	WT	80	0.013	0.055	0.230
3	WT	250	0.027	0.097	0.495
3	mut	5	0.036	0.807	3.286
3	mut	10	0.033	0.440	2.258
3	mut	40	0.013	0.091	0.224
3	mut	80	0.011	0.044	0.084
3	mut	250	0.014	0.067	0.137
4	WT	5	0.180	0.813	3.140
4	WT	10	0.095	0.443	1.732
4	WT	20	0.013	0.019	0.101
4	WT	40	0.009	0.019	0.072
4	WT	80	0.020	0.068	0.265
4	WT	250	0.019	0.060	0.254
4	mut	5	0.122	1.271	3.884
4	mut	10	0.072	1.031	3.537
4	mut	40	0.020	0.149	0.768
4	mut	80	0.049	0.431	1.596
4	mut	250	0.037	0.844	3.754

TABLE S10. α/k_{off} HBB

k	SNP	tet	low.HPD	median	upp.HPD
1	WT	5	180.624	213.178	250.384
1	WT	10	125.805	147.598	168.798
1	WT	20	216.330	261.287	314.761
1	WT	40	212.117	270.985	329.730
1	WT	80	214.432	257.880	304.762
1	WT	250	477.217	564.684	648.593
1	mut	5	9.080	10.960	13.174
1	mut	10	28.529	36.058	43.356
1	mut	40	44.662	57.687	71.459
1	mut	80	43.999	55.447	69.005
1	mut	250	59.522	70.628	84.777
2	WT	5	82.844	96.710	111.647
2	WT	10	118.521	142.328	186.000
2	WT	20	180.061	222.460	269.372
2	WT	40	256.229	310.385	368.848
2	WT	80	238.431	309.659	327.796
2	WT	250	481.478	561.546	649.773
2	mut	5	35.331	42.066	49.954
2	mut	10	38.750	55.886	71.052
2	mut	40	47.767	63.226	77.583
2	mut	80	72.672	93.342	115.105
2	mut	250	61.357	86.761	108.005
3	WT	5	69.549	81.039	94.196
3	WT	10	114.861	170.317	170.356
3	WT	20	124.441	164.157	206.865
3	WT	40	153.175	216.801	264.885
3	WT	80	141.653	180.708	226.265
3	WT	250	149.771	189.476	213.603
3	mut	5	29.455	35.547	42.080
3	mut	10	25.170	31.255	38.079
3	mut	40	34.828	47.958	60.944
3	mut	80	65.273	87.569	108.009
3	mut	250	95.857	119.091	143.867
4	WT	5	84.599	97.546	113.826
4	WT	10	104.599	123.292	142.147
4	WT	20	215.483	270.814	270.814
4	WT	40	249.124	305.273	366.964
4	WT	80	182.471	217.225	258.564
4	WT	250	234.660	281.937	339.927
4	mut	5	28.552	34.146	40.265
4	mut	10	30.453	37.481	44.636
4	mut	40	34.310	46.529	58.219
4	mut	80	30.063	38.528	47.509
4	mut	250	40.276	47.439	56.269

TABLE S11. κ HIV

k	SNP	tet	low.HPD	median	upp.HPD
1	WT	5	8.727	9.937	11.325
1	WT	10	10.993	12.288	13.592
1	WT	20	16.932	18.302	19.718
1	WT	40	18.385	19.903	20.011
1	WT	80	16.735	17.896	18.957
1	WT	250	24.550	25.974	27.432
1	mut	5	16.621	19.959	23.859
1	mut	10	21.241	23.881	27.318
1	mut	20	22.935	25.057	27.444
1	mut	40	19.246	20.688	22.178
1	mut	80	26.489	28.430	30.467
1	mut	250	24.061	25.942	27.678
2	WT	5	15.392	17.512	19.808
2	WT	10	25.774	28.301	30.527
2	WT	20	36.093	38.649	40.924
2	WT	40	34.004	35.801	37.798
2	WT	80	30.599	31.966	33.382
2	WT	250	37.518	39.354	41.293
2	mut	5	21.794	25.773	29.947
2	mut	10	43.278	47.496	52.058
2	mut	20	21.203	23.231	25.227
2	mut	40	30.657	32.984	35.508
2	mut	80	19.609	21.327	22.957
2	mut	250	16.493	17.664	18.954
3	WT	5	10.456	12.000	13.644
3	WT	10	9.830	10.997	12.398
3	WT	20	29.612	31.544	33.564
3	WT	40	15.692	16.768	17.845
3	WT	80	16.705	17.712	18.798
3	WT	250	19.341	20.192	21.265
3	mut	5	33.804	38.444	42.521
3	mut	10	29.922	32.648	36.088
3	mut	20	25.741	28.254	30.406
3	mut	40	21.824	23.662	25.236
3	mut	80	21.917	23.597	25.190
3	mut	250	16.718	17.810	18.906
4	WT	5	34.743	38.418	42.457
4	WT	10	37.419	40.703	43.863
4	WT	20	42.950	46.185	49.408
4	WT	40	48.250	51.426	54.571
4	WT	80	54.240	57.360	60.494
4	WT	250	53.328	56.927	60.132
4	mut	5	25.447	29.942	34.647
4	mut	10	34.322	38.062	42.392
4	mut	20	28.296	30.815	33.340
4	mut	40	26.199	28.116	29.970
4	mut	80	20.818	22.328	23.790
4	mut	250	20.302	21.626	22.973

TABLE S12. μ_X HIV gene

k	SNP	tet	low.HPD	median	upp.HPD
1	WT	5	67.005	72.838	79.536
1	WT	10	109.810	115.686	121.952
1	WT	20	144.574	151.166	157.431
1	WT	40	194.485	198.005	203.512
1	WT	80	226.244	232.415	238.770
1	WT	250	231.469	238.032	244.048
1	mut	5	31.686	37.672	43.353
1	mut	10	52.227	58.303	64.193
1	mut	20	89.312	95.185	101.282
1	mut	40	133.357	139.395	145.681
1	mut	80	156.590	162.956	169.112
1	mut	250	180.919	187.275	193.192
2	WT	5	66.834	73.001	78.969
2	WT	10	110.155	116.385	122.115
2	WT	20	146.758	152.367	157.963
2	WT	40	193.705	200.206	205.751
2	WT	80	226.944	232.737	238.957
2	WT	250	233.022	238.787	244.544
2	mut	5	33.431	38.818	44.292
2	mut	10	58.085	63.467	68.566
2	mut	20	88.921	95.219	101.320
2	mut	40	133.678	140.521	146.283
2	mut	80	155.778	162.631	168.680
2	mut	250	180.361	186.879	193.168
3	WT	5	67.657	73.147	79.668
3	WT	10	110.114	115.655	121.652
3	WT	20	145.713	152.053	157.986
3	WT	40	192.742	199.274	205.308
3	WT	80	226.620	233.022	238.193
3	WT	250	232.351	238.150	244.483
3	mut	5	36.811	40.994	45.435
3	mut	10	55.191	60.551	64.555
3	mut	20	89.503	95.670	101.158
3	mut	40	133.490	139.695	145.130
3	mut	80	156.822	162.594	169.538
3	mut	250	180.569	186.922	192.906
4	WT	5	69.528	75.142	81.061
4	WT	10	111.093	117.156	122.570
4	WT	20	146.982	153.429	159.127
4	WT	40	195.212	201.345	207.570
4	WT	80	229.161	235.061	241.236
4	WT	250	234.182	240.462	246.342
4	mut	5	34.228	39.432	44.903
4	mut	10	54.750	60.567	66.025
4	mut	20	89.372	95.749	101.674
4	mut	40	133.614	139.938	146.017
4	mut	80	156.317	162.691	168.913
4	mut	250	180.968	186.969	193.373

TABLE S13. $\tilde{k}_{on}$ HIV gene

k	SNP	tet	low.HPD	median	upp.HPD
1	WT	5	0.003	0.004	0.005
1	WT	10	0.003	0.004	0.005
1	WT	20	0.006	0.009	0.011
1	WT	40	0.009	0.012	0.016
1	WT	80	0.006	0.008	0.010
1	WT	250	0.009	0.012	0.015
1	mut	5	0.002	0.003	0.004
1	mut	10	0.003	0.004	0.005
1	mut	20	0.004	0.005	0.007
1	mut	40	0.007	0.009	0.011
1	mut	80	0.004	0.006	0.007
1	mut	250	0.004	0.005	0.007
2	WT	5	0.002	0.003	0.004
2	WT	10	0.004	0.005	0.007
2	WT	20	0.006	0.008	0.011
2	WT	40	0.008	0.012	0.015
2	WT	80	0.013	0.018	0.023
2	WT	250	0.010	0.014	0.019
2	mut	5	0.002	0.003	0.004
2	mut	10	0.004	0.005	0.006
2	mut	20	0.004	0.005	0.006
2	mut	40	0.004	0.005	0.007
2	mut	80	0.003	0.004	0.005
2	mut	250	0.004	0.005	0.006
3	WT	5	0.002	0.003	0.004
3	WT	10	0.002	0.003	0.004
3	WT	20	0.009	0.012	0.015
3	WT	40	0.007	0.010	0.012
3	WT	80	0.008	0.011	0.014
3	WT	250	0.008	0.011	0.014
3	mut	5	0.003	0.004	0.005
3	mut	10	0.003	0.004	0.005
3	mut	20	0.005	0.006	0.008
3	mut	40	0.005	0.006	0.008
3	mut	80	0.004	0.005	0.007
3	mut	250	0.006	0.008	0.010
4	WT	5	0.004	0.006	0.007
4	WT	10	0.004	0.006	0.007
4	WT	20	0.004	0.006	0.008
4	WT	40	0.005	0.007	0.009
4	WT	80	0.006	0.008	0.011
4	WT	250	0.004	0.006	0.008
4	mut	5	0.003	0.003	0.004
4	mut	10	0.004	0.005	0.006
4	mut	20	0.005	0.006	0.008
4	mut	40	0.005	0.007	0.009
4	mut	80	0.004	0.005	0.007
4	mut	250	0.006	0.008	0.010

TABLE S14. $\tilde{k}_{\text{off}}$ HIV gene

k	SNP	tet	low.HPD	median	upp.HPD
1	WT	5	0.144	0.881	2.155
1	WT	10	0.084	0.562	1.685
1	WT	20	0.229	0.744	1.857
1	WT	40	0.038	0.078	0.654
1	WT	80	0.015	0.031	0.060
1	WT	250	0.135	0.590	1.298
1	mut	5	0.073	0.454	1.354
1	mut	10	0.051	0.368	1.166
1	mut	20	0.018	0.140	0.616
1	mut	40	0.123	0.478	1.361
1	mut	80	0.014	0.024	0.042
1	mut	250	0.016	0.044	0.189
2	WT	5	0.103	0.570	1.574
2	WT	10	0.052	0.401	1.406
2	WT	20	0.023	0.151	0.667
2	WT	40	0.045	0.191	0.656
2	WT	80	0.047	0.204	0.605
2	WT	250	0.023	0.097	0.353
2	mut	5	0.022	0.201	0.769
2	mut	10	0.013	0.037	0.169
2	mut	20	0.007	0.011	0.017
2	mut	40	0.012	0.019	0.031
2	mut	80	0.009	0.014	0.021
2	mut	250	0.012	0.020	0.031
3	WT	5	0.068	0.611	2.029
3	WT	10	0.038	0.556	1.761
3	WT	20	0.096	0.582	1.690
3	WT	40	0.088	0.348	0.988
3	WT	80	0.037	0.374	1.164
3	WT	250	0.059	0.117	0.226
3	mut	5	0.015	0.120	0.623
3	mut	10	0.011	0.030	0.233
3	mut	20	0.015	0.088	0.720
3	mut	40	0.024	0.146	0.626
3	mut	80	0.010	0.017	0.026
3	mut	250	0.016	0.036	0.122
4	WT	5	0.103	0.649	1.825
4	WT	10	0.020	0.195	0.755
4	WT	20	0.014	0.038	0.156
4	WT	40	0.011	0.017	0.026
4	WT	80	0.017	0.036	0.091
4	WT	250	0.010	0.015	0.021
4	mut	5	0.037	0.288	0.992
4	mut	10	0.010	0.020	0.041
4	mut	20	0.011	0.020	0.035
4	mut	40	0.013	0.024	0.042
4	mut	80	0.007	0.010	0.014
4	mut	250	0.017	0.037	0.078

TABLE S15. α/k_{off} HIV

k	SNP	tet	low.HPD	median	upp.HPD
1	WT	5	67.863	83.165	98.742
1	WT	10	110.233	128.710	148.311
1	WT	20	66.024	75.388	86.230
1	WT	40	62.055	86.423	86.468
1	WT	80	125.449	163.587	197.794
1	WT	250	78.058	89.165	100.338
1	mut	5	31.371	40.575	50.588
1	mut	10	39.406	48.621	58.372
1	mut	20	53.780	65.401	80.227
1	mut	40	50.390	58.418	66.771
1	mut	80	102.514	128.589	150.897
1	mut	250	107.239	136.430	165.491
2	WT	5	78.383	92.406	106.888
2	WT	10	85.438	97.416	111.716
2	WT	20	69.807	83.687	101.449
2	WT	40	65.879	78.702	95.247
2	WT	80	49.412	61.013	75.818
2	WT	250	65.047	84.639	112.098
2	mut	5	34.809	44.291	54.536
2	mut	10	38.469	51.197	64.148
2	mut	20	82.526	102.341	124.937
2	mut	40	98.967	120.615	143.267
2	mut	80	152.628	182.466	213.368
2	mut	250	135.805	164.695	193.826
3	WT	5	95.847	112.554	131.718
3	WT	10	152.746	177.896	201.429
3	WT	20	50.485	58.166	66.866
3	WT	40	80.785	93.509	106.082
3	WT	80	87.801	99.460	133.676
3	WT	250	88.618	103.986	120.259
3	mut	5	28.936	36.907	43.947
3	mut	10	46.523	63.475	79.732
3	mut	20	44.259	56.383	76.276
3	mut	40	67.822	80.040	95.357
3	mut	80	114.493	141.460	169.534
3	mut	250	77.043	104.075	130.875
4	WT	5	50.970	59.826	68.217
4	WT	10	77.752	95.427	118.147
4	WT	20	99.153	128.960	158.025
4	WT	40	147.939	179.362	211.985
4	WT	80	113.452	149.386	180.708
4	WT	250	205.845	243.531	280.996
4	mut	5	33.166	41.173	49.774
4	mut	10	40.803	53.581	68.012
4	mut	20	53.655	70.015	87.576
4	mut	40	71.864	90.996	110.250
4	mut	80	132.897	162.495	192.626
4	mut	250	82.023	104.932	129.862

B. Negative binomial distribution

In contrast to the Poisson-beta model, the negative-binomial model directly encodes the ratio α/k_{off} as a single parameter, which is inferred with rather narrow credible intervals. Parsimony suggests that the negative-binomial model is a reasonable choice for the genes considered here, as it encodes for the most relevant kinetic parameters, viz., the average burst size α/k_{off} and the burst frequency k_{on}. Fig. S11 shows the parameters estimated from the negative-binomial model. The traces of the posteriors chains from each replicates were combined according to the consensus Monte Carlo procedure (see section S4 B) to obtain a representation of the consensus belief in Fig. S12.

The 90% HPD CIs and medians of the estimated parameters κ, μ_X, k_{on}, and α/k_{off} are reported in Tables S16–S19 (HBB gene) and Tables S20–S23 (HIV gene).

TABLE S16. κ HBB

k	SNP	tet	low.HPD	median	upp.HPD
1	WT	5	9.675	11.307	13.213
1	WT	10	22.041	25.232	28.377
1	WT	20	18.950	20.813	22.843
1	WT	40	20.381	22.383	24.447
1	WT	80	25.673	27.661	29.771
1	WT	250	17.300	18.830	20.649
1	mut	5	32.550	35.329	38.490
1	mut	10	16.072	18.688	21.615
1	mut	40	23.375	25.503	27.566
1	mut	80	27.251	30.309	34.188
1	mut	250	16.967	18.178	19.357
2	WT	5	23.578	26.572	29.961
2	WT	10	23.453	26.572	29.997
2	WT	20	21.562	23.610	25.909
2	WT	40	25.687	28.089	30.456
2	WT	80	31.358	33.931	36.457
2	WT	250	24.861	26.446	28.603
2	mut	5	26.626	29.697	33.019
2	mut	10	31.988	36.180	41.474
2	mut	40	40.925	44.272	47.412
2	mut	80	27.407	30.832	34.251
2	mut	250	22.856	24.409	26.037
3	WT	5	25.676	29.020	32.801
3	WT	10	32.162	35.936	39.914
3	WT	20	30.366	32.843	35.501
3	WT	40	30.841	33.200	35.696
3	WT	80	24.637	26.419	28.015
3	WT	250	20.441	21.780	23.367
3	mut	5	24.569	27.336	30.290
3	mut	10	42.637	47.605	52.771
3	mut	40	35.782	38.444	41.379
3	mut	80	31.078	35.045	38.636
3	mut	250	28.041	30.084	32.136
4	WT	5	17.636	20.198	23.004
4	WT	10	17.386	19.747	22.473
4	WT	20	21.240	23.109	25.149
4	WT	40	29.894	32.568	35.174
4	WT	80	29.411	31.375	33.856
4	WT	250	23.425	25.036	26.811
4	mut	5	14.236	15.954	17.716
4	mut	10	22.721	26.243	30.138
4	mut	40	32.983	35.546	38.257
4	mut	80	28.575	31.849	35.621
4	mut	250	26.358	27.852	29.440

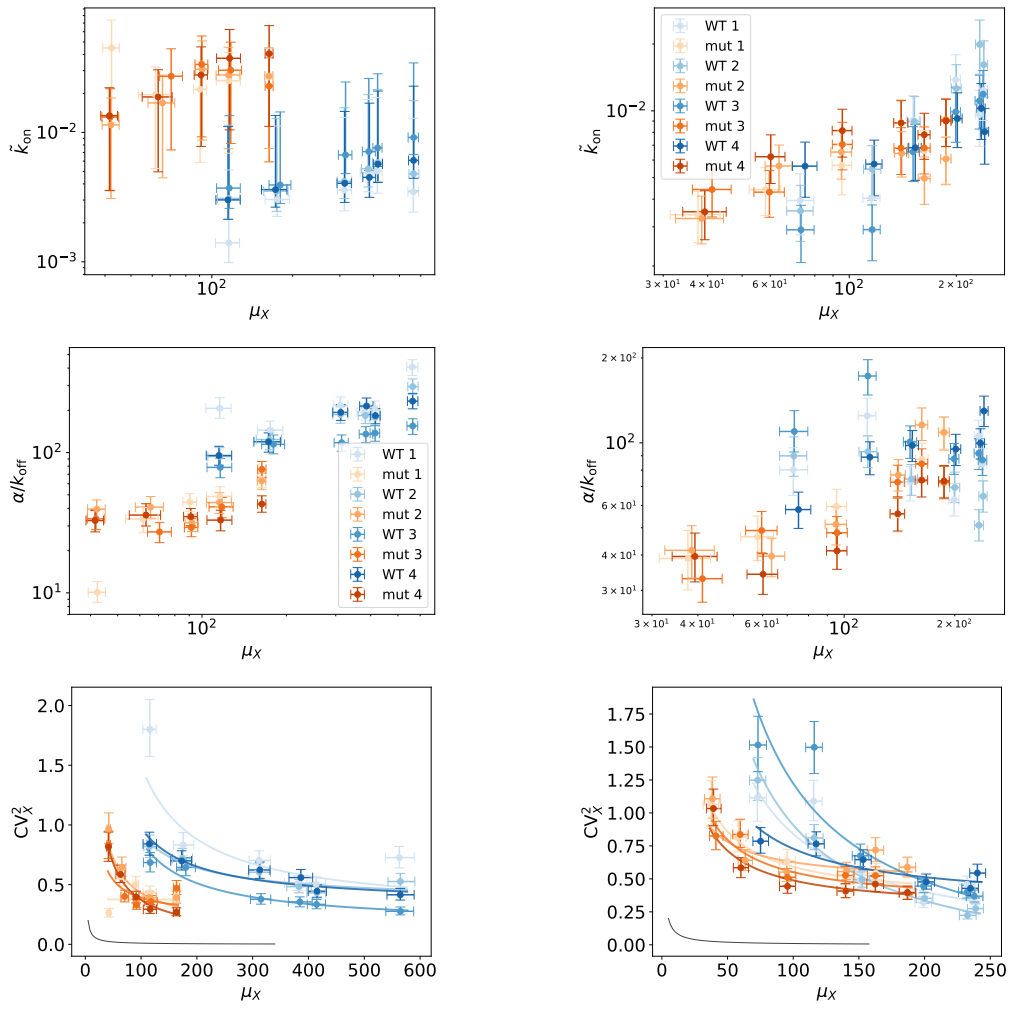

A HBB. **B** HIV.

FIG. S11. Estimates for parameters $\tilde{k}_{\text{on}}$, μ_X, and α/k_{off} of the negative-binomial model, from wild-type (blue) and mutant (orange) cell data, for all induction levels, shades of colors corresponds to replicates. Points are medians, error bars comprise 90% HPD CIs. HBB-gene results show consistent results across all the replicates (panel **A**). The HIV-gene results are reported in panels **B**. Results are consistent with the Poisson-beta model estimates (Fig. S9). Increasing expression levels, three replicates show a drop-off in the average burst size and an increase in the burst frequency, see also Fig. S2.

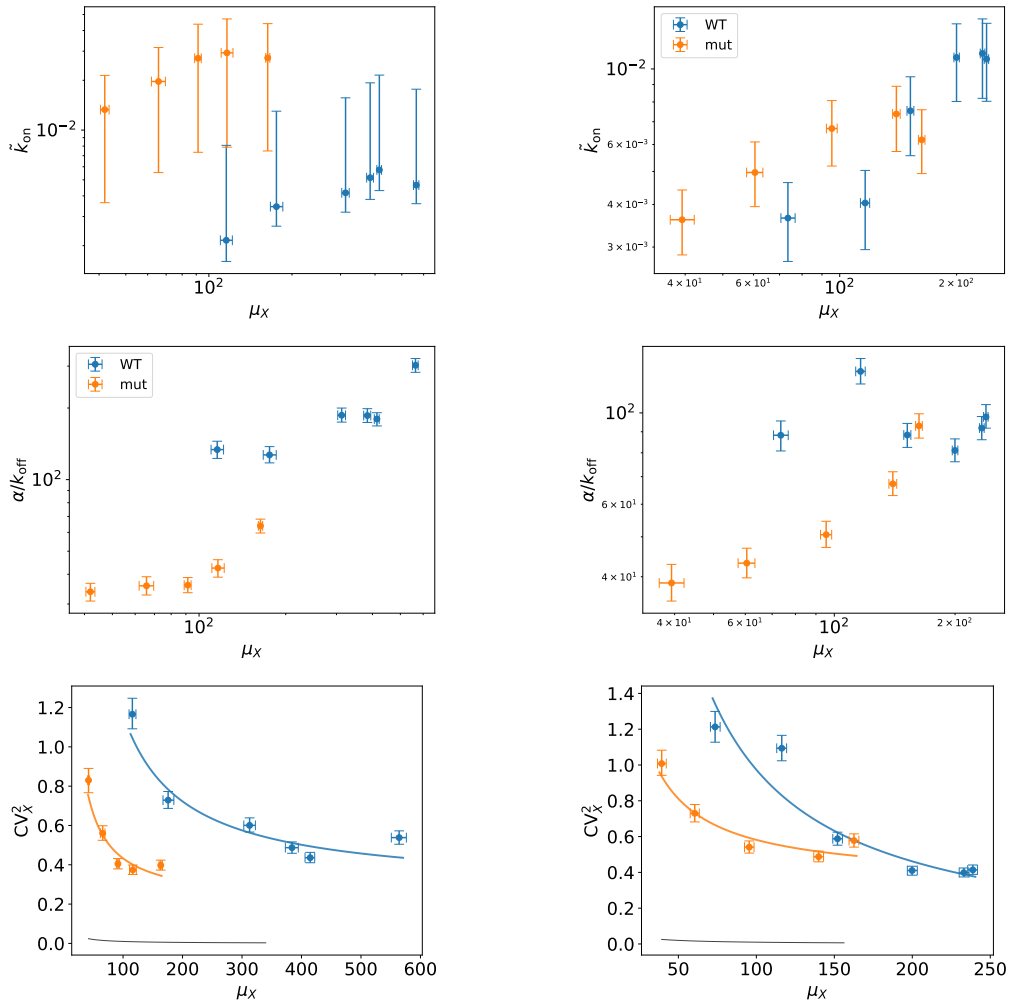

A HBB. **B** HIV.

FIG. S12. Consensus estimates of the parameters $\tilde{k}_{\text{on}}$, μ_X, and α/k_{off} from the negative-binomial model, from wild-type (blue) and mutant (orange) cell data, for all induction levels. Points are medians, error bars comprise 90% HPD CIs. HBB-gene results are in panel **A**, HIV-gene results are reported in panel **B**.

TABLE S17. μ_X HBB

k	SNP	tet	low.HPD	median	upp.HPD
1	WT	5	103.193	115.687	126.875
1	WT	10	157.904	175.269	194.327
1	WT	20	293.749	311.584	331.666
1	WT	40	357.077	382.068	402.882
1	WT	80	397.085	413.625	430.396
1	WT	250	537.710	562.996	589.504
1	mut	5	39.255	42.325	45.219
1	mut	10	53.368	61.634	69.735
1	mut	40	85.470	90.459	95.633
1	mut	80	103.857	115.778	127.620
1	mut	250	157.575	163.136	168.842
2	WT	5	104.884	115.671	127.339
2	WT	10	156.119	174.189	192.233
2	WT	20	292.999	311.784	331.770
2	WT	40	360.835	382.742	404.849
2	WT	80	397.159	414.805	430.893
2	WT	250	542.191	564.530	590.432
2	mut	5	39.031	42.105	45.158
2	mut	10	57.835	65.531	72.791
2	mut	40	86.987	92.086	96.961
2	mut	80	103.723	115.390	127.323
2	mut	250	157.508	163.312	168.777
3	WT	5	104.159	116.177	127.657
3	WT	10	163.259	179.811	197.030
3	WT	20	296.072	314.846	332.531
3	WT	40	363.753	384.298	406.525
3	WT	80	397.951	414.531	430.464
3	WT	250	538.464	564.609	588.360
3	mut	5	38.955	41.838	44.995
3	mut	10	63.927	70.558	77.724
3	mut	40	86.541	91.645	96.597
3	mut	80	105.958	117.686	129.102
3	mut	250	157.977	163.500	169.119
4	WT	5	103.541	114.909	127.623
4	WT	10	153.130	172.692	190.326
4	WT	20	292.635	312.606	330.812
4	WT	40	365.063	386.377	407.528
4	WT	80	399.614	415.485	432.185
4	WT	250	540.558	564.417	589.218
4	mut	5	38.556	41.557	44.534
4	mut	10	55.032	63.112	71.160
4	mut	40	85.960	91.252	96.281
4	mut	80	104.157	116.484	127.851
4	mut	250	157.935	163.479	169.027

TABLE S18. $\tilde{k}_{on}$ HBB

k	SNP	tet	low.HPD	median	upp.HPD
1	WT	5	0.001	0.001	0.005
1	WT	10	0.002	0.003	0.011
1	WT	20	0.003	0.004	0.013
1	WT	40	0.004	0.005	0.018
1	WT	80	0.004	0.005	0.019
1	WT	250	0.002	0.003	0.013
1	mut	5	0.012	0.045	0.074
1	mut	10	0.005	0.019	0.032
1	mut	40	0.006	0.021	0.035
1	mut	80	0.007	0.025	0.041
1	mut	250	0.007	0.027	0.044
2	WT	5	0.002	0.003	0.011
2	WT	10	0.003	0.004	0.013
2	WT	20	0.003	0.004	0.015
2	WT	40	0.004	0.005	0.019
2	WT	80	0.004	0.006	0.022
2	WT	250	0.003	0.005	0.018
2	mut	5	0.003	0.011	0.019
2	mut	10	0.005	0.017	0.027
2	mut	40	0.008	0.031	0.051
2	mut	80	0.007	0.028	0.045
2	mut	250	0.007	0.028	0.046
3	WT	5	0.003	0.004	0.014
3	WT	10	0.003	0.004	0.015
3	WT	20	0.005	0.007	0.025
3	WT	40	0.005	0.007	0.026
3	WT	80	0.005	0.008	0.027
3	WT	250	0.006	0.009	0.034
3	mut	5	0.003	0.013	0.021
3	mut	10	0.008	0.027	0.045
3	mut	40	0.009	0.033	0.054
3	mut	80	0.009	0.030	0.050
3	mut	250	0.006	0.023	0.038
4	WT	5	0.002	0.003	0.011
4	WT	10	0.003	0.004	0.013
4	WT	20	0.003	0.004	0.015
4	WT	40	0.003	0.005	0.017
4	WT	80	0.004	0.006	0.021
4	WT	250	0.004	0.006	0.022
4	mut	5	0.003	0.013	0.023
4	mut	10	0.005	0.019	0.031
4	mut	40	0.008	0.028	0.045
4	mut	80	0.010	0.037	0.063
4	mut	250	0.011	0.041	0.065

TABLE S19. α/k_{on} HBB

k	SNP	tet	low.HPD	median	upp.HPD
1	WT	5	175.298	206.600	246.085
1	WT	10	120.820	144.691	167.516
1	WT	20	190.560	217.633	249.246
1	WT	40	170.125	194.471	222.404
1	WT	80	181.291	206.076	232.972
1	WT	250	354.322	406.867	459.164
1	mut	5	8.579	10.098	12.020
1	mut	10	26.797	33.634	40.524
1	mut	40	38.121	44.326	50.962
1	mut	80	41.023	48.685	57.037
1	mut	250	56.503	64.628	73.724
2	WT	5	79.762	93.656	108.321
2	WT	10	104.729	123.788	143.569
2	WT	20	161.758	186.721	211.985
2	WT	40	160.712	183.674	208.313
2	WT	80	156.316	177.567	201.871
2	WT	250	258.811	295.198	334.765
2	mut	5	33.600	39.522	45.973
2	mut	10	34.079	40.868	48.606
2	mut	40	27.354	31.636	36.378
2	mut	80	36.745	44.057	51.733
2	mut	250	54.699	62.845	71.400
3	WT	5	66.198	78.414	90.605
3	WT	10	97.887	114.499	133.520
3	WT	20	102.297	117.574	133.503
3	WT	40	117.655	135.267	152.972
3	WT	80	120.396	137.453	155.178
3	WT	250	134.325	154.819	174.205
3	mut	5	28.241	33.741	39.190
3	mut	10	22.808	27.192	31.662
3	mut	40	25.141	29.293	33.804
3	mut	80	34.292	41.021	47.862
3	mut	250	66.549	75.912	86.434
4	WT	5	81.257	95.302	110.891
4	WT	10	100.651	119.384	138.147
4	WT	20	169.562	193.318	219.519
4	WT	40	187.460	214.568	244.764
4	WT	80	160.411	183.310	206.170
4	WT	250	204.957	232.671	264.311
4	mut	5	27.219	32.786	38.579
4	mut	10	29.960	35.848	43.176
4	mut	40	30.133	34.940	39.916
4	mut	80	27.685	33.007	38.815
4	mut	250	37.564	42.970	49.161

TABLE S20. κ HIV

k	SNP	tet	low.HPD	median	upp.HPD
1	WT	5	8.683	9.925	11.355
1	WT	10	10.830	12.201	13.502
1	WT	20	16.946	18.291	19.696
1	WT	40	17.995	19.136	20.300
1	WT	80	16.814	17.998	19.187
1	WT	250	24.456	25.898	27.413
1	mut	5	16.450	19.977	23.853
1	mut	10	20.826	23.864	27.041
1	mut	20	22.626	24.912	27.281
1	mut	40	19.162	20.677	22.160
1	mut	80	26.548	28.642	30.929
1	mut	250	24.056	26.022	27.857
2	WT	5	15.406	17.501	19.880
2	WT	10	25.483	28.210	30.905
2	WT	20	36.121	38.563	41.320
2	WT	40	33.654	35.716	37.949
2	WT	80	30.499	32.001	33.633
2	WT	250	37.389	39.279	41.400
2	mut	5	21.886	25.819	30.735
2	mut	10	42.808	47.476	52.389
2	mut	20	21.292	23.474	25.662
2	mut	40	30.748	33.257	35.874
2	mut	80	19.858	21.585	23.433
2	mut	250	16.597	17.858	19.331
3	WT	5	10.305	11.911	13.704
3	WT	10	9.759	10.994	12.394
3	WT	20	15.478	16.882	18.327
3	WT	40	15.642	16.744	17.818
3	WT	80	16.849	17.904	19.029
3	WT	250	19.059	20.252	21.472
3	mut	5	33.159	38.139	43.447
3	mut	10	28.905	32.666	36.895
3	mut	20	25.677	28.163	30.685
3	mut	40	21.877	23.641	25.428
3	mut	80	22.105	23.864	25.581
3	mut	250	16.736	17.863	19.027
4	WT	5	34.330	38.261	42.130
4	WT	10	37.272	40.394	44.002
4	WT	20	43.020	46.210	50.115
4	WT	40	48.515	51.534	54.970
4	WT	80	54.224	57.441	60.923
4	WT	250	54.376	57.496	61.232
4	mut	5	25.398	29.929	34.621
4	mut	10	34.261	38.357	42.825
4	mut	20	28.323	31.007	33.655
4	mut	40	26.348	28.262	30.242
4	mut	80	21.116	22.690	24.363
4	mut	250	20.337	21.627	23.114

TABLE S21. μ_X HIV

k	SNP	tet	low.HPD	median	upp.HPD
1	WT	5	66.749	72.714	79.573
1	WT	10	109.215	115.559	121.995
1	WT	20	144.952	151.119	157.583
1	WT	40	192.656	199.155	205.249
1	WT	80	225.999	232.337	238.487
1	WT	250	232.122	238.168	244.560
1	mut	5	31.397	37.570	43.353
1	mut	10	52.305	58.144	64.224
1	mut	20	89.505	95.336	101.545
1	mut	40	133.432	139.663	146.087
1	mut	80	156.547	162.818	169.259
1	mut	250	180.854	187.190	193.263
2	WT	5	66.749	72.966	79.146
2	WT	10	109.748	115.981	122.719
2	WT	20	145.901	152.450	158.287
2	WT	40	193.656	199.980	206.311
2	WT	80	226.495	232.703	239.197
2	WT	250	232.607	238.913	244.831
2	mut	5	32.501	38.487	44.321
2	mut	10	58.006	63.477	68.941
2	mut	20	88.766	95.055	101.497
2	mut	40	133.898	140.390	146.663
2	mut	80	156.238	162.667	168.835
2	mut	250	180.541	186.876	193.151
3	WT	5	66.720	73.187	79.646
3	WT	10	109.464	116.001	122.177
3	WT	20	144.933	151.139	157.537
3	WT	40	192.762	199.160	205.284
3	WT	80	225.811	232.428	238.252
3	WT	250	231.709	237.918	244.421
3	mut	5	36.242	41.159	46.565
3	mut	10	53.945	59.653	65.693
3	mut	20	89.646	95.617	102.024
3	mut	40	133.566	139.776	146.113
3	mut	80	156.555	162.557	168.787
3	mut	250	180.705	186.932	193.327
4	WT	5	69.298	75.131	81.160
4	WT	10	111.288	117.514	123.639
4	WT	20	146.956	153.289	159.350
4	WT	40	194.908	201.289	207.621
4	WT	80	228.382	234.962	240.972
4	WT	250	234.384	240.198	246.468
4	mut	5	34.044	39.263	45.106
4	mut	10	54.421	60.168	65.966
4	mut	20	89.558	95.636	101.791
4	mut	40	133.322	139.929	146.100
4	mut	80	156.024	162.534	168.737
4	mut	250	180.686	187.024	193.207

TABLE S22. $\tilde{k}_{on}$ HIV

k	SNP	tet	low.HPD	median	upp.HPD
1	WT	5	0.003	0.004	0.005
1	WT	10	0.003	0.004	0.005
1	WT	20	0.007	0.009	0.012
1	WT	40	0.010	0.014	0.018
1	WT	80	0.007	0.010	0.012
1	WT	250	0.009	0.012	0.016
1	mut	5	0.003	0.003	0.004
1	mut	10	0.003	0.004	0.006
1	mut	20	0.004	0.006	0.007
1	mut	40	0.007	0.009	0.011
1	mut	80	0.005	0.007	0.008
1	mut	250	0.005	0.006	0.008
2	WT	5	0.003	0.004	0.005
2	WT	10	0.004	0.005	0.007
2	WT	20	0.007	0.009	0.012
2	WT	40	0.009	0.013	0.016
2	WT	80	0.015	0.020	0.026
2	WT	250	0.011	0.016	0.021
2	mut	5	0.002	0.003	0.004
2	mut	10	0.004	0.006	0.007
2	mut	20	0.005	0.007	0.008
2	mut	40	0.005	0.006	0.008
2	mut	80	0.004	0.005	0.006
2	mut	250	0.005	0.006	0.008
3	WT	5	0.002	0.003	0.004
3	WT	10	0.002	0.003	0.004
3	WT	20	0.005	0.007	0.008
3	WT	40	0.007	0.010	0.013
3	WT	80	0.008	0.011	0.014
3	WT	250	0.009	0.012	0.016
3	mut	5	0.003	0.004	0.006
3	mut	10	0.003	0.004	0.005
3	mut	20	0.005	0.007	0.009
3	mut	40	0.005	0.007	0.009
3	mut	80	0.005	0.007	0.009
3	mut	250	0.007	0.009	0.011
4	WT	5	0.004	0.006	0.007
4	WT	10	0.004	0.006	0.007
4	WT	20	0.005	0.007	0.009
4	WT	40	0.007	0.009	0.012
4	WT	80	0.007	0.010	0.013
4	WT	250	0.006	0.008	0.010
4	mut	5	0.003	0.004	0.004
4	mut	10	0.005	0.006	0.008
4	mut	20	0.006	0.008	0.010
4	mut	40	0.007	0.009	0.011
4	mut	80	0.006	0.008	0.010
4	mut	250	0.007	0.009	0.011

TABLE S23. α/k_{on} HIV

k	SNP	tet	low.HPD	median	upp.HPD
1	WT	5	65.123	80.224	96.055
1	WT	10	105.447	124.804	144.056
1	WT	20	62.196	72.693	82.359
1	WT	40	55.029	62.855	71.783
1	WT	80	91.968	105.675	120.244
1	WT	250	73.419	84.125	95.301
1	mut	5	30.097	38.894	48.835
1	mut	10	38.247	46.466	55.041
1	mut	20	50.656	59.480	68.448
1	mut	40	48.290	55.669	63.965
1	mut	80	75.487	87.423	99.612
1	mut	250	95.084	108.486	123.429
2	WT	5	76.105	89.902	104.946
2	WT	10	81.737	93.017	105.950
2	WT	20	65.181	74.363	83.731
2	WT	40	61.362	69.436	78.737
2	WT	80	44.884	51.005	57.922
2	WT	250	56.796	64.669	73.245
2	mut	5	33.159	41.584	50.823
2	mut	10	33.516	39.641	45.896
2	mut	20	43.426	51.414	59.328
2	mut	40	67.491	76.908	87.220
2	mut	80	101.936	115.771	132.951
2	mut	250	94.257	109.003	123.450
3	WT	5	92.776	109.735	130.017
3	WT	10	147.773	172.554	197.158
3	WT	20	88.084	100.818	114.809
3	WT	40	77.288	87.747	99.551
3	WT	80	80.400	91.796	103.421
3	WT	250	76.617	86.925	98.877
3	mut	5	27.222	32.985	39.572
3	mut	10	40.746	48.876	57.111
3	mut	20	41.247	48.004	54.827
3	mut	40	63.647	72.555	83.277
3	mut	80	72.747	84.254	95.213
3	mut	250	63.329	72.322	82.431
4	WT	5	49.732	58.001	66.871
4	WT	10	77.064	88.972	100.832
4	WT	20	85.802	97.901	110.523
4	WT	40	83.077	94.987	107.236
4	WT	80	87.612	99.737	112.167
4	WT	250	114.176	129.687	146.438
4	mut	5	32.124	39.552	47.867
4	mut	10	29.015	34.206	40.406
4	mut	20	35.600	41.423	47.690
4	mut	40	48.680	56.041	64.317
4	mut	80	64.269	73.738	84.134
4	mut	250	63.794	73.262	83.058

TABLE S24. κ HBB

k	SNP	tet	low.HPD	median	upp.HPD
2	WT	5	260.821	267.314	273.981
2	WT	10	270.677	277.100	284.186
2	WT	20	298.204	304.307	311.348
2	WT	40	305.802	312.765	319.762
2	WT	80	321.045	327.146	334.050
2	WT	250	338.221	345.124	349.512
2	mut	5	165.515	172.460	179.105
2	mut	10	192.112	198.697	206.055
2	mut	40	183.042	189.718	196.109
2	mut	80	185.722	192.343	199.121
2	mut	250	178.993	185.852	192.476

TABLE S25. μ_{X} HBB

k	SNP	tet	low.HPD	median	upp.HPD
2	WT	5	11.310	11.728	12.148
2	WT	10	16.261	16.814	17.355
2	WT	20	23.646	24.285	25.005
2	WT	40	33.593	34.477	35.487
2	WT	80	42.511	43.591	44.589
2	WT	250	42.719	43.602	44.549
2	mut	5	7.300	7.704	8.128
2	mut	10	11.689	12.224	12.753
2	mut	40	21.350	22.256	23.111
2	mut	80	17.868	18.619	19.384
2	mut	250	21.277	22.220	23.121

C. Poisson distribution

The Poisson model encodes only one biological parameter, viz., the average gene expression level μ_X. We fitted this model to data from one of the replicates as a benchmark. The 90% HPD CIs and medians of the estimated parameters κ and μ_X, are reported in Tables S24–S25 (HBB gene) and Tables S26–S27 (HIV gene). It is worth noting that, compared to the prior derived in section S3 and both the estimates from the Poisson-beta and negative-binomial models of Tables S6, S11, S16, and S20, the κ is overestimated. In fact, high values of κ compensate for the small dispersion encoded in a Poisson random variable. Jointly with the fact that the Poisson model shows lower GoF than the two general models (subsection S4 C and figure S7), we conclude that the expression of the genes HIV and HBB is relative to a Poisson random variable and a flexible gene expression model for $X_i^{(k)}$, such as the Poisson-beta or the negative-binomial models, is necessary to exploit the measurement equation (24).

TABLE S26. CV_X^2 HBB

k	SNP	tet	low.HPD	median	upp.HPD
2	WT	5	0.082	0.085	0.088
2	WT	10	0.058	0.059	0.061
2	WT	20	0.040	0.041	0.042
2	WT	40	0.028	0.029	0.030
2	WT	80	0.022	0.023	0.024
2	WT	250	0.022	0.023	0.023
2	mut	5	0.123	0.130	0.137
2	mut	10	0.078	0.082	0.085
2	mut	40	0.043	0.045	0.047
2	mut	80	0.052	0.054	0.056
2	mut	250	0.043	0.045	0.047

TABLE S27. κ HIV

k	SNP	tet	low.HPD	median	upp.HPD
4	WT	5	245.093	251.782	258.632
4	WT	10	276.948	283.448	290.234
4	WT	20	291.102	297.690	304.497
4	WT	40	285.262	291.524	298.090
4	WT	80	300.678	306.854	313.563
4	WT	250	315.404	321.897	328.357
4	mut	5	172.173	179.215	186.314
4	mut	10	183.339	189.696	196.491
4	mut	20	178.477	185.104	191.728
4	mut	40	189.708	196.348	203.244
4	mut	80	183.321	189.823	196.490
4	mut	250	185.416	192.345	198.760

TABLE S28. μ_{X} HIV

k	SNP	tet	low.HPD	median	upp.HPD
4	WT	5	11.520	11.960	12.434
4	WT	10	17.091	17.645	18.199
4	WT	20	24.572	25.315	26.012
4	WT	40	37.049	38.005	39.049
4	WT	80	46.374	47.601	48.746
4	WT	250	45.807	46.889	48.064
4	mut	5	6.517	6.877	7.264
4	mut	10	12.027	12.547	13.114
4	mut	20	15.649	16.369	17.065
4	mut	40	19.839	20.665	21.484
4	mut	80	19.157	19.943	20.770
4	mut	250	20.907	21.769	22.651

TABLE S29. CV_X^2 HIV

k	SNP	tet	low.HPD	median	upp.HPD
4	WT	5	0.080	0.084	0.087
4	WT	10	0.055	0.057	0.058
4	WT	20	0.038	0.040	0.041
4	WT	40	0.026	0.026	0.027
4	WT	80	0.021	0.021	0.022
4	WT	250	0.021	0.021	0.022
4	mut	5	0.137	0.145	0.153
4	mut	10	0.076	0.080	0.083
4	mut	20	0.059	0.061	0.064
4	mut	40	0.047	0.048	0.050
4	mut	80	0.048	0.050	0.052
4	mut	250	0.044	0.046	0.048

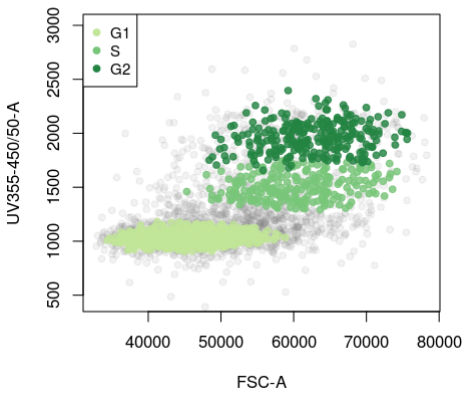

FIG. S13. Scatter plot of the `UV355-450/50-A` vs `FSC-A` signal for the 40 ng/mL Tet-induced HBB gene, replicate $k = 3$. Cells from the three phases, highlighted with different green-scale colors, were separated using flowClust.

S7. CELL CYCLE

Staining for DNA concentration allows us to heuristically find cells that are in G1, S, and G2 phases of the cell cycle, see Figs. S1(right) and S13. We considered the dataset with cells treated at concentration of 40 ng/mL of Tet. We separated the data points corresponding to the G1 phase from those from S and G2 using flowClust [4]. The less dense cluster S-G2 was further separated in two groups (corresponding to the phases S and G2) running the same algorithm again. Results are shown in Fig. S13 for HBB cell line, $k = 3$.

Data from phase G1, S, and G2 are referred to as $y^{(k)}_{\rm G1}$, $y^{(k)}_{\rm S}$, and $y^{(k)}_{\rm G2}$, respectively, for each replicate k. We refer to their averages (sample standard deviations of mean) as $\bar{y}_{\rm G1}$, $\bar{y}_{\rm S}$, and $\bar{y}_{\rm G2}$, ($s_{\bar{y}_{\rm G1}}$, $s_{\bar{y}_{\rm S}}$, and $s_{\bar{y}_{\rm G2}}$) respectively. To take into account that the mean gene expression seems to change with the cell phase, we introduce the conversion factors $c^{(k)} = \bar{x}/\bar{y}^{(k)}$ to obtain $\bar{x}^{(k)}_{\rm i} = c^{(k)}\bar{y}_{\rm i}$ and $s^{(k)}_{\bar{x}_{\rm i}} = c^{(k)}s_{\bar{y}_{\rm i}}$ which in turn are used in the informative priors

$$\mu^{(k)}_{X_{\rm i}} \sim \mathcal{N}(\bar{x}^{(k)}_{\rm i}, s^{(k)}_{\bar{x}_{\rm i}}), \tag{40}$$

${\rm i} = {\rm G1, S, G2}$. Equations (40) take the place of μ_X in the DAG of Fig. S5(B) for the G1, S, and G2 phase, respectively, for each replicate k. Fitting the negative-binomial model to 500 samples from each dataset yields the consensus estimates of Fig. 4(C-D) (*Main text*). In addition to this, we also subset reads form each phase into three groups by their size (based on the values of their FSC-A fluorescense signal, see *Main text*). We assume that the cell cycle and the cell size are extrinsic contributors to the total transgene mRNA variability, with the remaining variability sources thought of as being intrinsic. As in Ref. [8], using the symbol $\langle\cdot\rangle_{\rm I}$ for the average over the intrinsic variables, with the cell phase held fixed, and $\langle\cdot\rangle_{\rm E}$ for the average over the different cell phases, the law of total variance allows us to write, for the mRNA abundance X,

$${\rm CV}^2_X = \frac{\langle\langle X^2\rangle_{\rm I} - \langle X\rangle^2_{\rm I}\rangle_{\rm E}}{\langle\langle X\rangle_{\rm I}\rangle^2_{\rm E}} + \frac{\langle\langle X\rangle^2_{\rm I}\rangle_{\rm E} - \langle\langle X\rangle_{\rm I}\rangle^2_{\rm E}}{\langle\langle X\rangle_{\rm I}\rangle^2_{\rm E}}, \tag{41}$$

where the first term on the r.h.s. is the intrinsic noise, while the second term is the extrinsic noise. Computing the two terms gives the intrinsic and extrinsic noise levels of Tables S30 and Fig. 4(D) (*Main text*), which show that the cell cycle and the cell size always contributed only a minor term to the total noise.

TABLE S30. Intrinsic noise, extrinsic noise and total noise from each replicate of wild-type HBB and HIV genes, 40 ng/mL Tet. First table is based on cell-phase only partition, second table is bases on both cell phase and cell size. Extrinsic noise has the lowest contribution to the total noise.

gene	k	intr. noise	extr. noise	tot. noise
HBB	1	0.587	0.017	0.060
HBB	2	0.399	0.033	0.014
HBB	3	0.380	0.023	0.008
HBB	4	0.448	0.024	0.030
HIV	1	0.322	0.053	0.015
HIV	2	0.417	0.041	0.020
HIV	3	0.444	0.040	0.029
HIV	4	0.289	0.036	0.021

gene	k	intr. noise	extr. noise	tot. noise
HBB	1	0.514	0.025	0.539
HBB	2	0.467	0.054	0.521
HBB	3	0.381	0.020	0.401
HBB	4	0.477	0.023	0.500
HIV	1	0.324	0.044	0.369
HIV	2	0.423	0.039	0.461
HIV	3	0.492	0.039	0.531
HIV	4	0.301	0.029	0.330

S8. POLII-MEDIATED 3'-5' INTERACTIONS BY CHIA-PET

We considered scRNAseq and ChIA-PET data accessible at the GEO Series numbers GSE124682 [23] and GSE33664 [24], respectively.

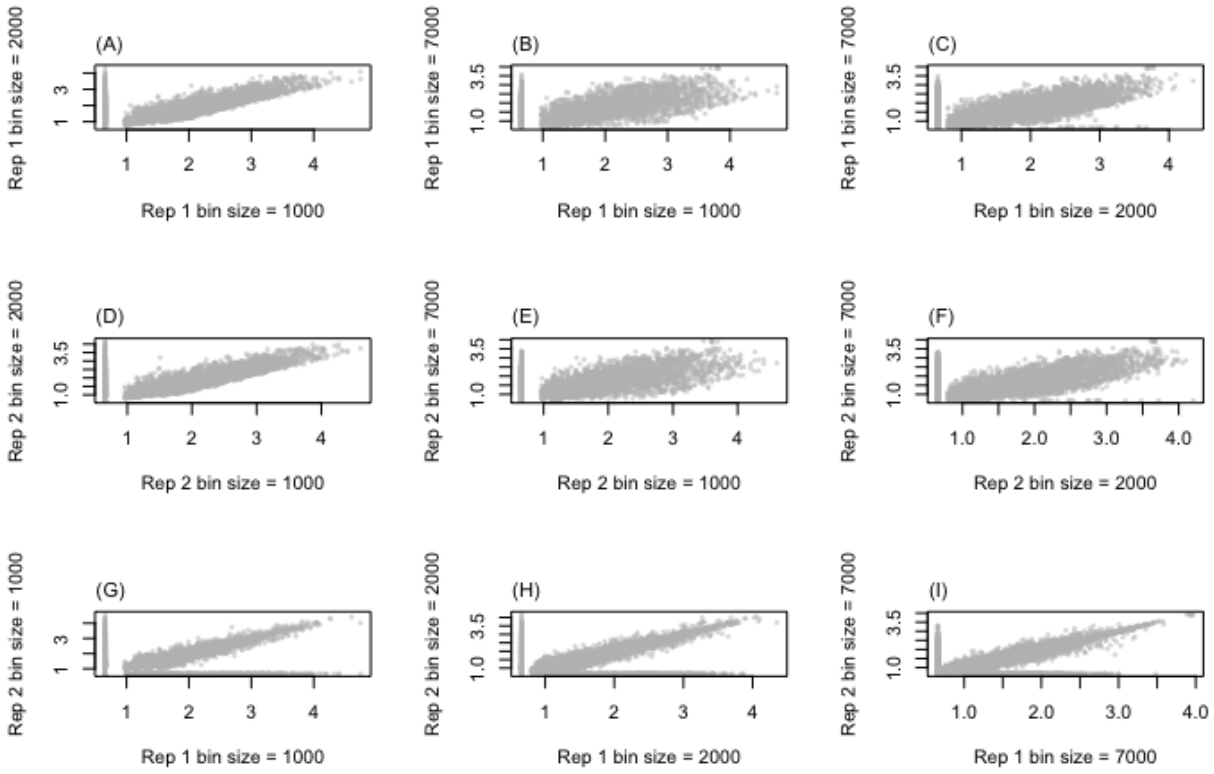

FIG. S14. Joint plots of 3'-5' interaction scores. For each biological replicate (Rep 1 and Rep 2, corresponding to GSM832464 and GSM832465, respectively), the interaction scores obtained at different bin resolutions (1, 2, and 7 Kbs) appear strongly correlated. (G)-(I) Similarly, the two biological repeats appear strongly correlated at each bin resolution.

Raw chromatin contact frequency is highest for small genomic distances. In order to normalise for this and expose deviations from this general relationship, we need to divide by the expected number of reads at a given genomic distance. We calculate this by random sampling 10000 genomic intervals and measuring the contact frequency over this sample. This estimate appears robust to decreasing the number of sampled intervals. The relation between gene length and the normalised 3'-5' interaction score is illustrated in Fig. S15. Genes with length smaller than the resolution of the interaction matrices are discarded from the main analysis.

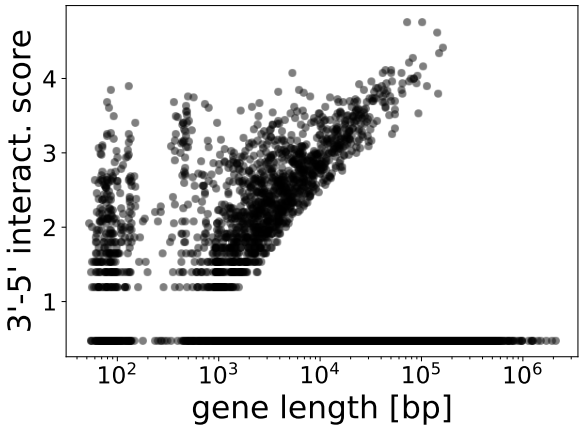

FIG. S15. 3'-5' interaction score vs gene length. The cluster corresponding to small lengths mostly includes pseudo-genes.

We fitted the model of equations (54)–(56) to the smRNAseq data, thus enabling a convenient classification of genes based on transcription; see also, e.g., reference [25]. Without correction for incomplete capture of mRNA, the parameter $\bar{k}_{\rm on}$ incorporates here both biological and technical above-Poisson noise, whilst allowing the ranking of the genes based on their total noise.

S9. MICROSCOPIC GENE EXPRESSION MODEL

We referred to the models of section S2 as the phenomelogical models. In fact, our main concern there was to exploit a minimal description of the statistics of the transcription events and the stationary mRNA distribution—which is the (observed) phenomenology, indeed. Due to their simplicity, these models allowed us to attain the important goal of separating the technical noise (due to background fluorescence and measurement process) from the biological noise encoded into X_i.

Nevertheless, there are specific microscopic biological mechanisms, more difficult to observe, that may give rise to the observed phenomena. In our tetracycline-inducible genes, Tet repressor (TetR) homodimers bind to the operator $TetO_2$ downstream of the transcription start site (TSS). When such a binding event occurs, the transcription is inhibited as the elongation is impeded. Adding Tet in turn alters the conformation of TetR and hinders the binding events, having the net effect of inducing the gene expression. Crucially, during the "on" phase, the transcription rate is proportional to the abundance of PolII (law of mass action), which can be thought of as waiting in a compartment upstream of the TSS [26]. Therefore, when the gene is actively transcribing, its rate can vary in time according to the amount of PolII ready to initiate transcription. After transcription, PolII can either be re-injected into the compartment and set ready for a new initiation event (PolII recycling), or disposed into the nuclear environment. Also, the compartment recruits PolII from the nuclear environment. This can be described by means of the following chemical reaction scheme:

$$\varnothing \xrightarrow{\gamma} \text{PolII}, \tag{42}$$

$$\text{DNA}_{\text{on}} + \text{PolII} \xrightarrow{l\,\beta} \text{mRNA} + \text{DNA}_{\text{on}} + \text{PolII}, \tag{43}$$

$$\text{DNA}_{\text{on}} + \text{PolII} \xrightarrow{(1-l)\,\beta} \text{mRNA} + \text{DNA}_{\text{on}}, \tag{44}$$

$$\text{DNA}_{\text{on}} \xrightarrow{\lambda_{\text{off}}} \text{DNA}_{\text{off}}, \tag{45}$$

$$\text{DNA}_{\text{off}} \xrightarrow{\lambda_{\text{on}}} \text{DNA}_{\text{on}}, \tag{46}$$

$$\text{mRNA} \xrightarrow{d} \varnothing, \tag{47}$$

$$\text{PolII} \xrightarrow{\delta} \varnothing, \tag{48}$$

where DNA_{on} and DNA_{off} are unlocked and locked DNA configurations, respectively. The presence of the 3'-5' crosstalk loop is thought to facilitate the recycling of PolII after each transcription event; therefore we can study the effect of the recycling on the simulated expression data by tuning l in the reaction scheme. Obviously, the pA mutation lowers the recycling probability l with respect to the WT, but l is not supposed to be zero in mutant genes, as the recycling can occur by means of other mechanisms (e.g., diffusion). By the law of mass action

$$\lambda_{\text{off}} = nK_\lambda, \tag{49}$$

$$\lambda_{\text{on}} = K_\lambda, \tag{50}$$

where K_λ is a chemical affinity and n is the concentration of TetR. Hence, we can imitate variations in the Tet dose by fine-tuning n, with large values of Tet (high induction levels) corresponding to small values of n. Unlike the simpler phenomenological models, we do not have an analytical likelihood for this model, thus parameter inference is more challenging, to be addressed with likelihood-free methods. We simulate the model using the Doob-Gillespie algorithm; sample trajectories of mRNA abundances are plotted in Fig. 5 D (*Main text*).

When all the chemical species are highly abundant and the gene is always in "on" state (this can be achieved in the limit as $k_{\text{off}} \to 0$), it is straightforward to derive the following rate equations,

$$\frac{\mathrm{d}}{\mathrm{d}t}[\text{PolII}] = \alpha - [\text{PolII}](\delta - \beta(1-l)), \tag{51}$$

$$\frac{\mathrm{d}}{\mathrm{d}t}[\text{mRNA}] = [\text{PolII}]\beta - [\text{mRNA}]d, \tag{52}$$

where $[X]$ is the abundance of the species X. The stationary mRNA abundance is then

$$[\text{mRNA}] = \frac{\beta}{d}\frac{\alpha}{\delta + \beta(1-l)}, \tag{53}$$

which corresponds to the vertical lines of Fig. 4 B (*Main text*). While the parameters γ, β, d, δ, K_λ are chosen to simulate mRNA abundances and noises in ranges consistent with those of the real data, fine-tuning the recycling probability and the induction parameters l and n yields patterns similar to those observed in the experimental setting (i.e., those of Figs. S9, S11, and 2 (*Main text*)). More specifically, a simple scatter plot of the sample averages versus the CV^2 of [mRNA] shows a drift of the noise curve from the Poisson case $\text{CV}^2_X = 1/\mu_X$ as the recycling rate l increases. Fitting a negative binomial (NB) Bayesian model

$$\text{mRNA} \sim \text{NB}(\mu_X, k_{\text{on}}), \tag{54}$$

$$\mu_X \sim \text{Gamma}(0.001, 0.001), \tag{55}$$

$$k_{\text{on}} \sim \text{Gamma}(0.001, 0.001), \tag{56}$$

to 500 simulated stationary mRNA abundances, allowed us to estimate the average burst size $\alpha/k_{\text{off}} = \mu_X/k_{\text{on}}$ and the burst frequency k_{on} shown in Figs. S16 and 5 C (*Main text*).

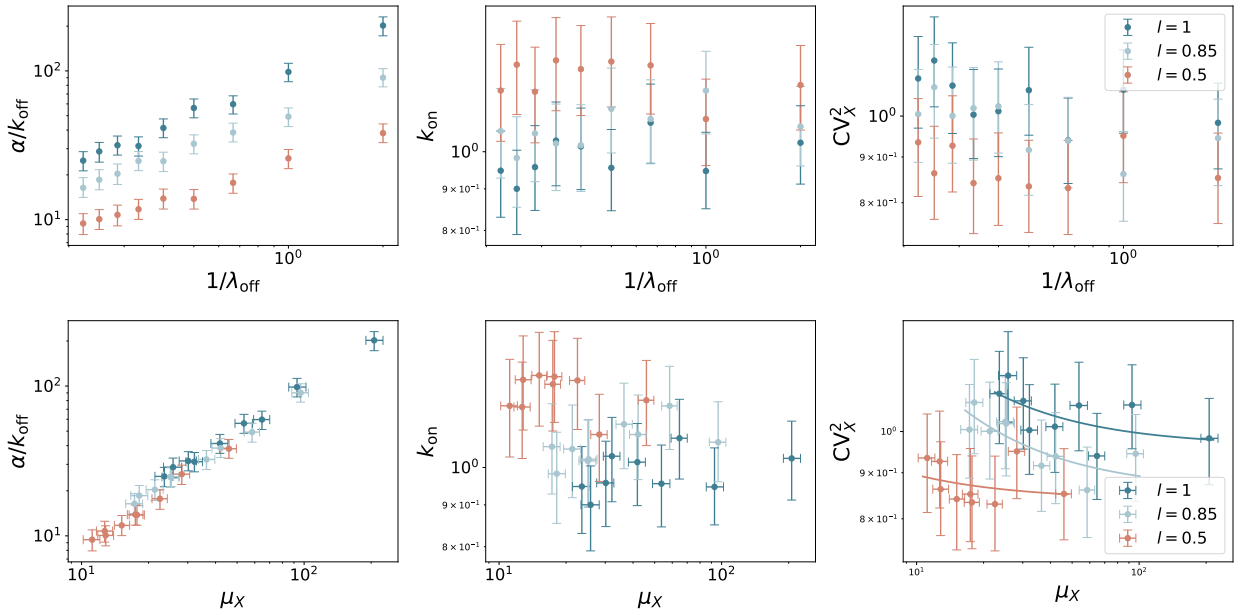

FIG. S16. Negative-binomial model fit to 500 mRNA abundances simulated from the microscopic model. The pattern of the inferred average burst sizes and burst frequencies mirrors those obtained from the real data. For each value of the recycling probability l ($l = 0.5, 0.85, 1$), simulations are performed with $\lambda_{off} = 0.5, 1, 1.5, 2, 2.5, 3, 2.5, 3.5, 4, 4.5$; remaining parameters are $(\gamma, \beta, d, \delta, \lambda_{on}) = (10, 10, 0.01, 1, 0.01)$. The solid lines in the noise plot (lower-left plot) are fitted $CV_X^2 = A/\mu_X + B$ curves.

S10. MATERIALS

A. Cell lines and cell culture

The wildtype HBB and HIV-1-*env* cell lines have been utilized in previous studies [22, 27, 28]. The nomenclature was changed for the present manuscript, with the cell lines denoted HBB WT, HBB mut, HIV WT and HIV mut, which had been denoted β pA+, β pA−, HIV-1 pA+ and HIV-1 pA− in [22], respectively. Cells were maintained in DMEM medium supplemented with 10% fetal bovine serum and 100 μg mL^{-1} penicillin-streptomycin (DMEM-10). Induction of cell lines was carried out for 16 hours before downstream experiments.

Deletion cell line construction. The design and construction of the deletion cell line used the protocol detailed in [29], with the following changes. A dual sgRNA strategy was employed with a 5' guide binding between the AmpR promoter and CMV enhancer and a 3' guide binding just after the 3' FRT site. The use of plasmid pSpCas9(BB)-2A-GFP (PX458) and dual targeting necessitated the transfection with two plasmids, each containing a respective guide. Transfection was carried out using calcium phosphate, followed by washing the cells with warm PBS after 16-24 hours and replacing the media. Cells were allowed to recover for 48-72 hours before single-cells were isolated in 96-well plates via FACS (BD ARIAFusion), with the brightest 10% GFP positive cells being sorted. Testing for deletion was initially verified via genomic DNA extraction and PCR, followed by smFISH assay using flow cytometry.

B. Single-molecule RNA fluorescence in situ hybridization

Probe sets. Probe sets for HBB and HIV-1-*env* RNA were designed with the tool at www.biosearchtech.com/stellarisdesigner (see Table S31 for sequences). The probe sets were synthesized by LGC Biosearch Technologies as custom Stellaris® probe sets. AKT1 probes were ready-made and ordered from LGC Biosearch.

smFISH. smFISH staining followed the probe manufacturer's protocol. Briefly, cells were grown on poly-L-lysine treated glass coverslips overnight, fixed in 3.7% formaldehyde for 10 minutes and permeabilized in ethanol for $>$ 1 hour. After overnight staining at 37°C in dextran sulphate and formamide buffered with SSC, cells were washed, followed by mounting onto a slide using Vectashield with DAPI as the mounting medium. Imageing was carried out

TABLE S31. Sequences and details of smFISH probe sets. Product Name: Stellaris® FISH Probes, Custom Assay with Quasar® 670 Dye.

1) Oligo Name: HIV

```
tcactaaacgagctcgtcga ggtcaaaacagcgtggatgg
taaacgctagagtccggagg gagctcggtaccaagcttaa
agaattccaccacactggac cagcagttgttgcagaatta
ctatgtcgacacccaattct tctgtcgagtaacgcctatt
agtctaggatctactggagg tggtacaagcagttttaggc
ggcaatgaaagcaacacttt cctaaggcttttgtcatgaa
gagtctgactgttctgatga gctgctttgatagagaagct
cttcttcttctattccttcg aggatccgttcactaatcga
cagatcgtcccagataagtg tagctgaagaggcacaggct
agagtaagtctctcaagcgg ttccacaatcctcgttacaa
aatatttgagggcttcccac ccaatactgtaggagattcc
gcactattctttagttcctg ctgtggcattgagcaagtta
cttctataaccctatctgtc agctctataagctgcttgta
tattcttctaggtatgtggc agcaaaatcctttccaagcc
tacttttgaccacttgcca ttacagcaggccatccaatc
ctcagctcgtctcattcttt cctctagactcgagatactg
gctgatcagcgggtttaaac ctggcaactagaaggcacag
accttccagggtcaaggaag taggaaaggacagtgggagt
```

2) Oligo Name: HBB

```
tcactaaacgagctcgtcga aaacagcgtggatggcgtct
cggtgtcttctatggaggtc tttaaacgctagagtccgga
gtcagaagcaaatgtaagct ggttgctagtgaacacagtt
tgcaccatggtgtctgtttg gcagtaacggcagacttctc
caacttcatccacgttcacc aaagaacctctgggtccaag
gagtggacagatccccaaag cttagggttgcccataacag
gagcactttcttgccatgag caggccatcactaaaggcac
cttgaggttgtccaggtgag cactcagtgtggcaaaggtg
acgtgcagcttgtcacagtg agcctgaagttctcaggatc
aaagtgatgggccagcacac ctggtggggtgaattctttg
caccactttctgataggcag cgcttagtgatacttgtggg
tggacagcaagaaagcgagc cttagggaacaaaggaacct
tagacccagtttggtagttg tcatgttttctacagctaga
tccagcagacatgggtgatc tcctcatgttttctacagtc
ctagacagcagacatgggtg gtgatcctcatgttttctac
tacagtcgtccagcagacat atgggtgatcctcatgtttt
ttctacagctagacagcaga agacatgggtgatcctcatg
ctcatgttttctacagtcgt tagacagcagacatgggtga
ttatctagatccggtggatc ttgtggtttgtccaaactca
gcatttttttcactgcattc tgcagcttataatggttaca
gcaattgttgttgttaactt
```

on a brightfield microscope.

Flow cytometry. DNA staining was carried out with FxCycle™ Violet Stain (ThermoFisher, F10347) at a concentration of 1 μg mL^{-1}. Fixed cells were analysed on a BD Fortessa. Processing and data analysis of raw flow cytometry data was carried out using the flowcore R package [1] (v1.48, R version 3.3).

SmFISH spot counting. Quantification of RNA was carried out using FISH-quant [30]. Images were imported with the following settings: XY 64.8 nm; Z 200 nm; Refractive index 1.515; NA 1.40; Em 592; Ex 546; Microscope widefield. Cell outlines were drawn manually. A single image was then processed and the settings used to batch-process the remaining set. The *threshold* and *quality score* parameters of FISH-quant were set to quantify as many spots as possible while reducing spurious detection through batch-specific selection of these parameters.

C. RNA isolation and preparation, and degradation rate estimation

Total RNA was extracted from the respective cell lines following the RNeasy Mini Kit (Qiagen, 47104) protocol, using QIAshredder (Qiagen, 79654). RNA for RNA-seq analysis was treated with TURBO DNA-*free*™ kit (ThermoFisher, AM1907).

To estimate the mRNA degradation rate, RNA was reverse transcribed using random primers (Promega, C118A) and M-MLV reverse transcriptase (Promega, M170A) followed by qPCR using SensiMix™ SYBR® No-Rox (Bioline, QT650-02) on a Qiagen Rotor-Gene Q. Gene-specific primers were used (HIV Forward `TCTCCTACGGCAGGAAGAAG`; HIV Reverse `GGTAGCTGAAGAGGCACAGG`). Analysis was carried out by calculating the CT values using the qpcR R package [31] (v1.4-1) and from this $2^{-\Delta\Delta Ct}$ were calculated using the mut time 0 concentration as the reference sample. A degradation time series was carried out by standard induction method at 250 ng mL^{-1} tetracycline for 16 hours, followed by removal of media and washing with warm DMEM-10. Cells were then placed in fresh medium and samples were taken at different time points following on from this.

D. Nanostring

Cells were seeded, induced and processed as indicated previously (subsection S10 A), with the following alteration: after trypsinisation cells were resuspended in 1 mL of PBS and kept on ice. Counting of cells was carried out via Countess (ThermoFisher) cell counter with 100 μL (50 : 50) PBS to trypan blue. Samples were spun down at 500 g for 5 minutes and were then resuspended in RLT buffer from RNeasy Mini Kit (Qiagen, 47104) with beta-mercaptoethanol to obtain a concentration of 6500 cells per μL. Samples were then vortexed for 1 minute and placed at -80°C. Cell lysis was verified under a microscope. Samples were shipped on dry ice to an external provider for processing. Custom probe sets, including probes targeting HIV-1-*env* along with GAPDH and AKT1 as house-keeping genes, were designed and shipped by NanoString Technologies.

E. RNA-seq

Library preparation. RNA-seq libraries were prepared using 500 ng of total input RNA and the NEBNext® UltraTM II Directional RNA Library Prep Kit for Illumina (E7760L), along with the NEBNext® rRNA Depletion Kit (E6310L) and NEBNext® Multiplex Oligos for Illumina Set 1 and 2 (E7335, E7500). Ribo-depletion was carried out to capture transgene RNA regardless of the absence or presence of a poly(A) tail. The manufacturer's manual was followed, with the final PCR amplification using 9 cycles. Libraries were assessed via Bioanalyser, diluted and mixed before being sequenced on an Illumina® NextSeq 500, generating paired-end reads with read length 42.

RNA-seq analysis. Data quality control was performed with FastQC v0.11.5. Read and adapter trimming was carried out using TrimGalore! v0.4.3 with cutadapt v0.4.3 using default settings [32]. Indices for STAR to map to were constructed from the human genome (GRCh38.p12, Gencode primary annotation) and the respective (HBB WT/mut and HIV-1-*env* WT/mut) transgenic sequence. The GTF was modified to include these genes as a separate chromosome (chrHBB or chrHIV). To mask the existing HBB sequence, bedtools' (v2.25.0) `maskfasta` command was used [33]. RNA-seq reads were mapped to the genome using STAR software v2.5.3a with parameter `--outSAMattributes XS` [34]. Counts per gene were calculated using LiBiNorm [35] acting in an HTSeq-count [36] compatible mode with the following parameters: `--format=bam --minaqual=10 --stranded=reverse --mode=intersection-strict`. Coverage statistics were generated using deepTools' (v3.1.3) `bamCoverage` [37]. Fold changes for the HBB and HIV genes were calculated using DESeq2 v1.22.1 [38] from Bioconductor release 3.8 and R v3.5.1.

Splicing analysis. To analyse potential alternative splicing in the *env* transgene, BAM files were imported into R (v4.0.2) and analysed using SGSeq (v1.4) [39]. A table of counts relating to potential splice variants (Table S32) indicates that there are potential alternative splicing events, however the number of reads related to each variant indicates that they are present across all samples and appear related to the overall abundance of mRNA. To further analyse the difference between introns and exons in the HIV-1 env wild-type and mutant cell lines, the Transcripts Per Kilobase Million (TPM), a normalisation that takes account of both sequence depth and gene length, were calculated (Fig. S17). BAM files were imported into R (v4.0.2) and analysed using Rsubread (v2.2.6) [40], calling `FeatureCounts` with the following parameters: `minOverlap=20`, `isPairedEnd=TRUE`, `strandSpecific=2`. We do see a slightly higher fraction of intronic reads present in the *env* mutant at 250 ng mL^{-1} Tet, although the principal difference between the mutant and wild-type appears to be overall mRNA abundance. In addition to this, ref. [22] quantified the levels of HBB pre-mRNA relative to the total HBB RNA and determined that ratios are the same within the first 2 hours of induction (splicing was slightly effected after 24 hours, albeit this phenotype appeared to arise subsequent to RNAPII depletion).

TABLE S32. Counts of potential splice variants in *env* transgene.

variantID	mut 0	mut 0	mut 0	mut 250	mut 250	mut 250	WT 0	WT 0	WT 0	WT 250	WT 250	WT 250
1	0	0	0	0	0	0	0	0	0	0	1	0
2	28	21	14	233	164	223	42	46	44	404	434	303
3	28	24	27	46	51	58	31	27	45	33	28	45
4	0	0	0	0	0	0	0	0	0	0	0	1
5	26	30	22	42	51	59	36	33	44	32	23	48
6	0	0	0	0	0	1	0	0	0	0	1	0
7	41	53	31	41	56	65	49	46	60	36	30	54
8	0	0	0	0	0	0	0	0	0	0	1	0
9	0	0	0	1	0	1	0	0	0	1	4	1
10	0	0	0	0	1	0	0	0	0	0	0	0

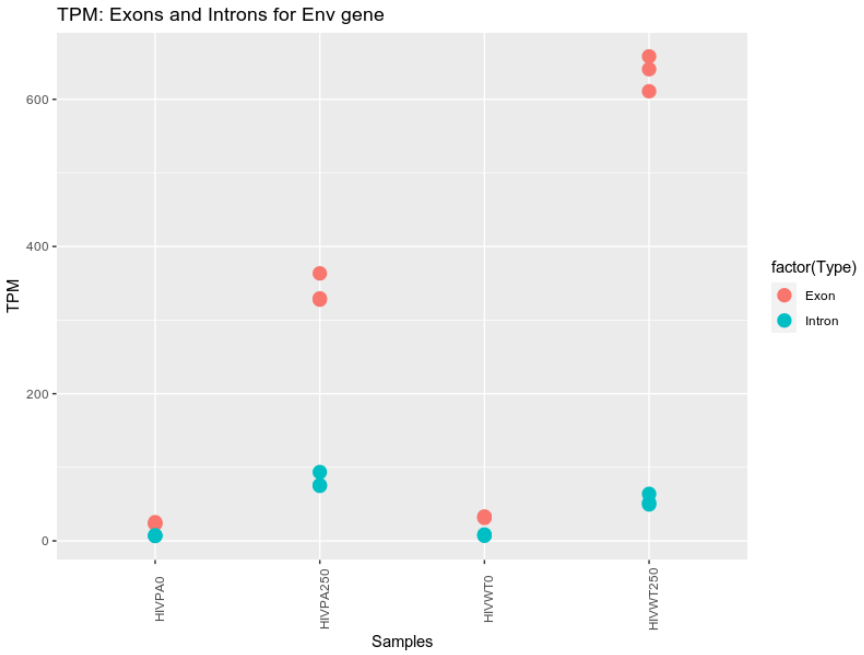

FIG. S17. TPMs of exonic and intronic regions in *env* transgene.

[1] F. Hahne, N. LeMeur, R. R. Brinkman, B. Ellis, P. Haaland, D. Sarkar, J. Spidlen, E. Strain, and R. Gentleman, BMC Bioinformatics **10**, 106 (2009).

[2] H. M. Shapiro, *Practical Flow Cytometry* (John Wiley & Sons, Inc., Hoboken, NJ, USA, 2003) pp. 1–733.

[3] K. Lo, R. Brinkman, and R. Gottardo, Cytometry A (2008).

[4] K. Lo, F. Hahne, R. Brinkman, and R. Gottardo, BMC Bioinformatics (2009), R package version 3.5.0.

[5] B. Munsky, G. Neuert, and A. van Oudenaarden, Science **336**, 183 (2012).

[6] J. Kim and J. C. Marioni, Genome Biology **14**, R7 (2013).

[7] S. Tiberi, M. Walsh, M. Cavallaro, D. Hebenstreit, and B. Finkenstädt, Bioinformatics **34**, i647 (2018).

[8] M. B. Elowitz, A. J. Levine, E. D. Siggia, and P. S. Swain, Science **297**, 1183 (2002).

[9] J. R. S. Newman, S. Ghaemmaghami, J. Ihmels, D. K. Breslow, M. Noble, J. L. DeRisi, and J. S. Weissman, Nature **441**, 840 (2006).

[10] A. Bar-Even, J. Paulsson, N. Maheshri, M. Carmi, E. O'Shea, Y. Pilpel, and N. Barkai, Nature Genetics **38**, 636 (2006).

[11] R. D. Dar, B. S. Razooky, L. S. Weinberger, C. D. Cox, and M. L. Simpson, PLoS ONE **10**, 1 (2015).

[12] M. Soltani, C. A. Vargas-Garcia, D. Antunes, and A. Singh, PLoS Computational Biology **12**, e1004972 (2016).

[13] M. Dobrzynski and F. J. Bruggeman, Proceedings of the National Academy of Sciences **106**, 2583 (2009).

[14] E. Meinelt, M. Reunanen, M. Edinger, M. Jaimes, A. Stall, D. Sasaki, and J. Trotter, *Standardizing Application Setup Across Multiple Flow Cytometers Using BD FACSDiva^{TM} Version 6 Software* (2012).

[15] C. Zechner, J. Ruess, P. Krenn, S. Pelet, M. Peter, J. Lygeros, and H. Koeppl, Proceedings of the National Academy of Sciences **109**, 8340 (2012).

[16] D. Adler, "vioplot: Violin plot," (2005), https://cran.r-project.org/package=vioplot.

[17] D. J. Spiegelhalter, K. R. K. R. Abrams, and J. P. Myles, *Bayesian approaches to clinical trials and health-care evaluation* (John Wiley & Sons, 2004) p. 391.

[18] A. Patil, D. Huard, and C. Fonnesbeck, Journal of Statistical Software **35**, 1 (2010).

[19] H. Haario, E. Saksman, and J. Tamminen, Bernoulli **7**, 223 (2001).

[20] S. L. Scott, A. W. Blocker, F. V. Bonassi, H. A. Chipman, E. I. George, and R. E. McCulloch, International Journal of Management Science and Engineering Management **11**, 78 (2016).

[21] O. Tange, ;login: The USENIX Magazine **36**, 42 (2011).

[22] C. K. Mapendano, S. Lykke-Andersen, J. Kjems, E. Bertrand, and T. H. Jensen, Molecular Cell **40**, 410 (2010).

[23] A. M. Klein, L. Mazutis, I. Akartuna, N. Tallapragada, A. Veres, V. Li, L. Peshkin, D. A. Weitz, and M. W. Kirschner, Cell **161**, 1187 (2015).

[24] G. Li, X. Ruan, R. K. Auerbach, K. S. Sandhu, M. Zheng, P. Wang, H. M. Poh, Y. Goh, J. Lim, J. Zhang, H. S. Sim, S. Q. Peh, F. H. Mulawadi, C. T. Ong, Y. L. Orlov, S. Hong, Z. Zhang, S. Landt, D. Raha, G. Euskirchen, C.-L. Wei, W. Ge, H. Wang, C. Davis, K. I. Fisher-Aylor, A. Mortazavi, M. Gerstein, T. Gingeras, B. Wold, Y. Sun, M. J. Fullwood, E. Cheung, E. Liu, W.-K. Sung, M. Snyder, and Y. Ruan, Cell **148**, 84 (2012).

[25] A. J. Larsson, P. Johnsson, M. Hagemann-Jensen, L. Hartmanis, O. R. Faridani, B. Reinius, Å. Segerstolpe, C. M. Rivera, B. Ren, and R. Sandberg, Nature **565**, 251 (2019).

[26] W.-K. K. Cho, N. Jayanth, B. P. English, T. Inoue, J. O. Andrews, W. Conway, J. B. Grimm, J.-H. H. Spille, L. D. Lavis, T. Lionnet, and I. I. Cisse, eLife **5** (2016), 10.7554/eLife.13617.

[27] C. K. Damgaard, S. Kahns, S. Lykke-Andersen, A. L. Nielsen, T. H. Jensen, and J. Kjems, Molecular Cell **29**, 271 (2008).

[28] A. B. Eberle, S. Lykke-Andersen, O. Mühlemann, and T. H. Jensen, Nature Structural and Molecular Biology **16**, 49 (2009).

[29] F. A. Ran, P. D. Hsu, J. Wright, V. Agarwala, D. A. Scott, and F. Zhang, Nature Protocols **8**, 2281 (2013).

[30] F. Mueller, A. Senecal, K. Tantale, H. Marie-Nelly, N. Ly, O. Collin, E. Basyuk, E. Bertrand, X. Darzacq, and C. Zimmer, Nature Methods **10**, 277 (2013).

[31] A. Spiess, "qpcR: Modelling and Analysis of Real-Time PCR Data," (2013), https://CRAN.R-project.org/package=qpcR.

[32] M. Martin, EMBnet.journal **17**, 10 (2011).

[33] A. R. Quinlan and I. M. Hall, Bioinformatics **26**, 841 (2010).

[34] A. Dobin, C. A. Davis, F. Schlesinger, J. Drenkow, C. Zaleski, S. Jha, P. Batut, M. Chaisson, and T. R. Gingeras, Bioinformatics **29**, 15 (2013).

[35] N. P. Dyer, V. Shahrezaei, and D. Hebenstreit, PeerJ **7**, e6222 (2019).

[36] S. Anders, P. T. Pyl, and W. Huber, Bioinformatics **31**, 166 (2015).

[37] F. Ramírez, F. Dündar, S. Diehl, B. A. Grüning, and T. Manke, Nucleic Acids Research **42**, W187 (2014).

[38] M. I. Love, W. Huber, and S. Anders, Genome Biology **15**, 550 (2014).

[39] L. D. Goldstein, Y. Cao, G. Pau, M. Lawrence, T. D. Wu, S. Seshagiri, and R. Gentleman, PLOS ONE **11**, e0156132 (2016).

[40] Y. Liao, G. K. Smyth, and W. Shi, Nucleic Acids Research **47**, e47 (2019).